The diverse roles of integrin α3β1 in cancer: Lessons learned from skin and breast carcinogenesis

Ramovš, V.

INTEGRIN α3β1 IN HAIR BULGE STEM CELLS MODULATES CCN2 EXPRESSION AND PROMOTES SKIN TUMORIGENESIS

Published in Life Science Alliance, Volume 3, number 7 (2020)

Veronika Ramovs[1], Ana Krotenberg Garcia[1#], Ji-Ying Song[2], Iris de Rink[3], Maaike Kreft[1], Roel Goldschmeding[4], Arnoud Sonnenberg[1]

1 Division of Cell Biology, The Netherlands Cancer Institute, Amsterdam, the Netherlands
2 Department of Experimental Animal Pathology, The Netherlands Cancer Institute, Amsterdam
3 Genomics Core Facility, The Netherlands Cancer Institute, Amsterdam, the Netherlands
4 Department of Pathology, UMC Utrecht, Utrecht, the Netherlands
#Current address: Division of Molecular Pathology, The Netherlands Cancer Institute, Amsterdam

Correspondence to Arnoud Sonnenberg: a.sonnenberg@nki.nl

ABSTRACT

Epidermal-specific deletion of integrin α3β1 almost completely prevents the formation of papillomas during DMBA/TPA two-stage skin carcinogenesis. This dramatic decrease in tumorigenesis was thought to be due to an egress and premature differentiation of α3β1-depleted hair bulge stem cells (HB SCs), previously considered to be the cancer cells-of-origin in the DMBA/TPA model. Using a reporter mouse line with inducible deletion of α3β1 in HBs, we show that HB SCs remain confined to their niche regardless of the presence of α3β1 and are largely absent from skin tumors. However, tumor formation was significantly decreased in mice deficient for α3β1 in HB SCs. RNA sequencing of HB SCs isolated from short-term DMBA/TPA-treated skin showed α3β1-dependent expression of the matricellular protein connective tissue growth factor (CCN2), which was confirmed in vitro, where CCN2 promoted colony formation and 3D growth of transformed keratinocytes. Together, these findings show that HBs contribute to skin tumorigenesis in an α3β1-dependent manner and suggest a role of HB SCs in creating a permissive environment for tumor growth through the modulation of CCN2 secretion.

INTRODUCTION

Hair bulge (HB) contains one of the most studied and characterized stem cell (SC) compartments in mammalian skin. Located at the bottom of the hair follicles (HFs) in the resting stage of hair cycle (i.e. telogen), it is the main reservoir for cells that form elongated HFs during the growth phase of hair cycle called anagen [1–3]. The transient-amplifying progeny of HB SCs normally remains confined within HFs, however, under specific circumstances some of these cells can egress and contribute to the interfollicular epidermis (IFE). Such behavior has been observed during wound-healing, when HB keratinocytes migrate out of their niche into the newly formed epidermis [4,5].

It has been suggested that HB SCs also play a crucial role in cutaneous skin tumorigenesis. An increased expression of HB marker keratin 19 (K19) has been observed in human squamous cell carcinomas (SCCs) [6], while basal cell carcinomas and trichoblastomas were shown to upregulate the expression of the HB marker keratin 15 (K15) [7]. Furthermore, several studies have suggested that HB SCs represent the cells-of-origin of papillomas, benign tumors that can progress into invasive SCCs and are formed during the two-stage chemically induced mouse skin carcinogenesis protocol (DMBA/TPA treatment) [8–11]. The suggestion that HB SCs play a crucial role in DMBA/TPA-induced carcinogenesis was also made in our previously reported study in mice, lacking integrin α3β1 in epidermis (K14 Itga3 KO mice). Integrin α3β1 is a transmembrane receptor for laminins-332 and -511 in the epidermal basement membrane and functions as bi-directional signaling molecule [12,13]. Upon its epidermal deletion, mice exhibit an increased epidermal turnover, which coincides with the loss of label-retaining cells and, importantly, with the localization of K15-positive keratinocytes in IFE and upper parts of HFs (i.e. isthmus and infundibulum) [14]. As K14 Itga3 KO mice showed a near absence of DMBA/TPA-induced tumorigenesis, we hypothesized that this could be due to the egress of DMBA-primed K15-positive HB SCs and their loss through squamous differentiation in IFE [14]. However, the HB origin of DMBA/TPA-derived tumors is somewhat controversial. Recent studies reported a limited contribution of HB SCs to papillomas [15], and demonstrated the importance of SCs residing in isthmus instead [16]. Furthermore, it has been reported that K15 promoter, which is widely used to generate genetic deletions in HB SCs, also targets basal cells in IFE, isthmus and infundibulum [9] and, importantly, that K15 can be miss-expressed during tumorigenesis, reflecting the activity and responsiveness of basal epidermal cells to the loss of skin homeostasis [17]. Considering all this, we found it important to re-evaluate the mechanisms behind the absence of tumorigenesis in K14 Itga3 KO mice. Here, we exploit linage tracing and next-generation sequencing analysis of a mouse model with

inducible deletion of α3β1 in HBs to investigate the role of α3β1 in HB SCs and their contribution to skin tumorigenesis.

RESULTS

HB keratinocytes lacking integrin α3β1 stay confined within their niche and contribute normally to hair cycle

In order to target and visualize HB SCs and their progeny, we generated a mouse line, expressing an inducible Cre (CreER) under the HB-specific K19 promoter (K19-CreER) [18] in combination with mT/mG reporter transgene [19] (K19 Itga3 WT mice). To investigate the role of α3β1 in HB SCs, we have further introduced floxed Itga3 alleles to our mouse model (K19 Itga3 KO mice) (**Fig. 1a**), which resulted in an efficient deletion of α3β1 in Cre-induced GFP-positive cells (**Fig. 1b**). Tamoxifen administration induced GFP expression in the majority of HFs in both K19 Itga3 KO and WT mice (**Supplementary Fig. 1a**) and, as expected, the GFP-positive cells localized to HBs, with no obvious leakiness detected (**Fig. 1c-e**). Surprisingly, linage tracing of HB cells, induced in the first telogen phase of the hair cycle (P21), showed that HB SCs remain confined to their niche, regardless of the presence of α3β1, and do not egress into infundibulum and/or IFE (**Fig. 1c and e, Supplementary Fig. 1b**), as was expected based on previously reported observations of K15-positive cells in the IFE of mice with an epidermis-specific deletion of α3β1 (K14 Itga3 KO mice) [14]. Furthermore, linage tracing during the first hair cycle revealed that Itga3 KO and WT HB cells contribute to all layers of growing HFs, with no observed differences in hair cycle progression between K19 Itga3 KO and WT mice (**Fig 1e**). Taken together, these data demonstrate that α3β1 plays no major role in HBs of adult mice under homeostatic conditions.

Epidermal deletion of α3β1 causes *de novo* expression of K15 outside of HBs

The finding that HB cells do not egress from their niche into the IFE of K19 Itga3 KO mice casted doubt on whether the K15-positive cells, previously observed in the IFE of K14 Itga3 KO mice, truly originate from HBs [14]. To re-evaluate their origin, we turned to the K14 Itga3 KO and WT mouse models (**Fig. 2a**). In accordance with previous work on this mouse model, immunostaining of whole-mount tail epidermis from K14 Itga3 KO mice confirmed the presence of K15-positive and α3β1-depleted keratinocytes in isthmus, infundibulum and IFE [14] (**Fig. 2b**). Remarkably, we observed that α3β1-positive cells that had escaped Cre-recombinase in K14 Itga3 KO mice preferentially localized to HBs in both tail and back skin (**Fig. 2b, c**). We confirmed this non-stochastic localization with flow cytometry, which showed that the remaining α3-positive keratinocytes isolated from back epidermis of K14 Itga3 KO mice were twice more likely to originate from HBs compared to their counterpart isolated from WT mice (**Fig. 2d, Supplementary Fig. 2a**).

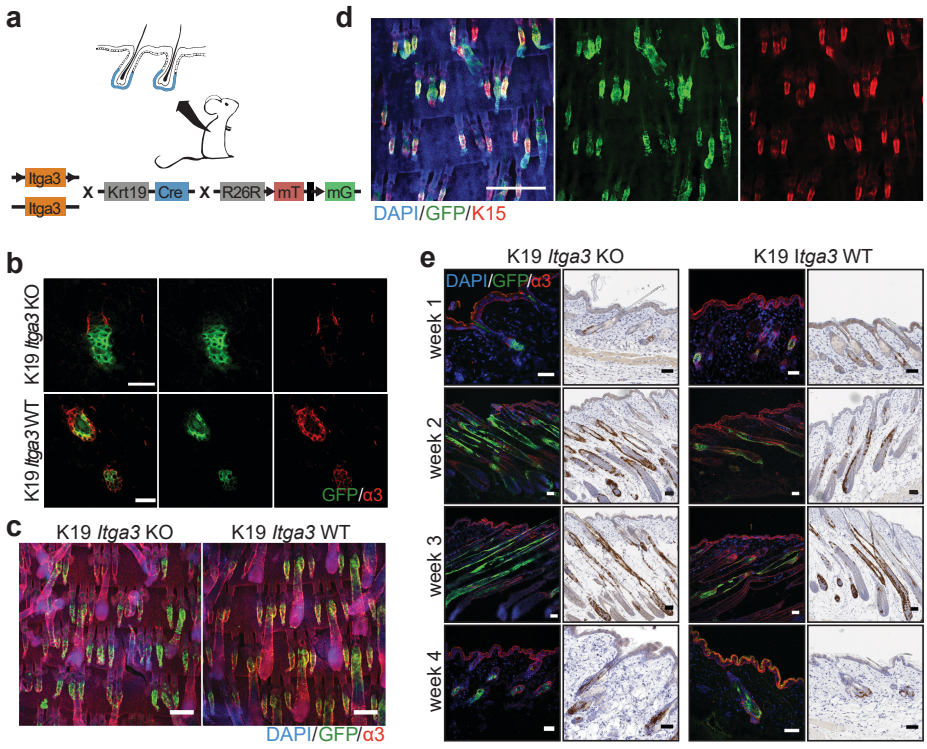

Figure 1: HB keratinocytes lacking integrin α3β1 stay confined within their niche and contribute normally to hair cycle. (**a**) Overview of the K19 Itga3 KO and WT mouse models. (**b**) Integrin α3β1 is expressed in Cre-induced GFP-positive keratinocytes of K19 Itga3 WT mice and efficiently deleted in GFP-positive keratinocytes of 7-week-old K19 Itga3 KO mice one week after tamoxifen treatment (back skin, scale bar: 30 μm). (**c**) Linage tracing of GFP-positive HB keratinocytes showing localization within their niche in K19 Itga3 KO and WT mice one week after tamoxifen treatment (whole mounts of tail epidermis, scale bar: 200 μm). Linage tracing of up to four weeks can be found in Supplementary figure S1b. (**d**) Whole mount of tail epidermis of K19 Itga3 WT mouse showing colocalization of Cre-induced GFP – positive cells and K15 marker in HBs (scale bar: 500 μm). (e) Linage tracing of GFP-positive HB SCs Cre-induced in telogen (P21) and followed for up to four weeks over whole hair cycle (until P49) in the back skin of K19 Itga3 KO and WT mice. Representative images of two to three mice per condition are shown (scale bar: 50 μm).

The relatively inefficient deletion of α3β1 in HBs in K14 Itga3 KO mice together with the absence of miss-localized HB keratinocytes in K19 Itga3 KO mice suggests that the loss of α3β1 in HB SCs does not lead to their egress, but rather that the miss-localized K15-positive keratinocytes originate from other epidermal compartments of K14 Itga3 KO mice. In order to determine whether K15 in these cells could be expressed de novo upon α3β1 deletion, we performed RT-qPCR of the RNA, isolated from tail and back epidermis of K14 Itga3 KO and WT mice. Indeed, an increased expression of K15 could be detected in the epidermis of K14 Itga3 KO, compared to WT mice (**Fig. 2e**), despite the absence of proliferating K15-positve cells residing in HBs (**Supplementary Fig.**

2b). We further confirmed that the miss-localized K15-positive keratinocytes were not derived from HB SCs by performing a quantitative flow cytometry analysis of the HB population size (CD34+, α6high), which was comparable between K14 Itga3 KO and WT mice (**Supplementary Fig. 2c, d**). This remained true even after mice were submitted to the short-term DMBA/TPA treatment, mimicking the initiation stage of tumorigenesis, during which an increased miss-localization of K15-positive keratinocytes had been previously reported for K14 Itga3 KO mice [14] (**Supplementary Fig. 2c, d**). All in all, this data strongly suggests that keratinocytes in IFE and upper parts of HFs express K15 de novo in the absence of α3β1 and provides new evidence that HB SCs remain confined within their niche regardless of whether they express α3β1.

The contribution of HB keratinocytes to newly formed IFE is increased in the absence of α3β1

The egress of HB SCs into IFE normally occurs during wound-healing, when HB keratinocytes contribute to the formation of neo-epidermis [4,5]. To test whether our model reflects these characteristics of HB SCs and to determine whether the presence of α3β1 affects induced egress of HB keratinocytes, we performed wounding experiments of K19 Itga3 KO and WT mice. The presence of α3β1 in HBs did not affect the closure of the wounds; no differences were observed in the length of neo-epidermis three days after the wounding and in the percentage of closed wounds five days after wounds were inflicted (**Fig. 3a, b**). As expected, Cre-induced, GFP-positive HB keratinocytes contributed to the formation of neo-epidermis upon wounding of both K19 Itga3 KO and WT mice (**Fig. 3c, d**). Whereas at the beginning of the wound re-epithelization no obvious differences in the contribution of HB-originating cells to the neo-epidermis could be observed between K19 Itga3 KO and WT mice (**Fig. 3c**), there was a small, but significant increase in the number of GFP-positive cells in the neo-epidermis of K19 Itga3 KO mice at the final stages of wound closure (**Fig. 3d**). This is consistent with previous observations that the absence of α3β1 promotes cell migration during wound-healing [20]. Together, these findings indicate that during wound healing, the egress of HB SCs into the neo-epidermis increases when α3β1 is absent from HB keratinocytes, which, however, does not alter the rate of re-epithelization.

The absence of α3β1 in HBs reduces susceptibility of mice to DMBA/TPA-mediated tumorigenesis

Next, we investigated the role of HB SC-residing α3β1 in skin carcinogenesis by submitting K19 Itga3 KO and WT mice to the complete DMBA/TPA carcinogenesis protocol. Tumors could be detected six weeks after the beginning of the treatment (P91-P97), regardless of the presence of α3β1 (**Fig. 4a**). Even though both, K19 Itga3 KO and WT mice developed numerous tumors by the end of the treatment (K19 Itga3

KO 33,8 and WT 49,1 tumors on average), there was a marked 30% decrease in tumor formation and a 15% decrease in the average tumor size upon the deletion of Itga3 in HB SCs (**Fig. 4a-b, Supplementary fig. 3a**). In line with this, K19 Itga3 KO mice exhibited significantly lower tumor burden compared to WT mice (K19 Itga3 KO 1313,5 and WT 2296,1 mm2 on average, **Fig. 4a**). Nearly all the tumors were benign papillomas and keratoacanthomas, with no notable difference in their prevalence between the two mouse lines (**Fig. 4c**).

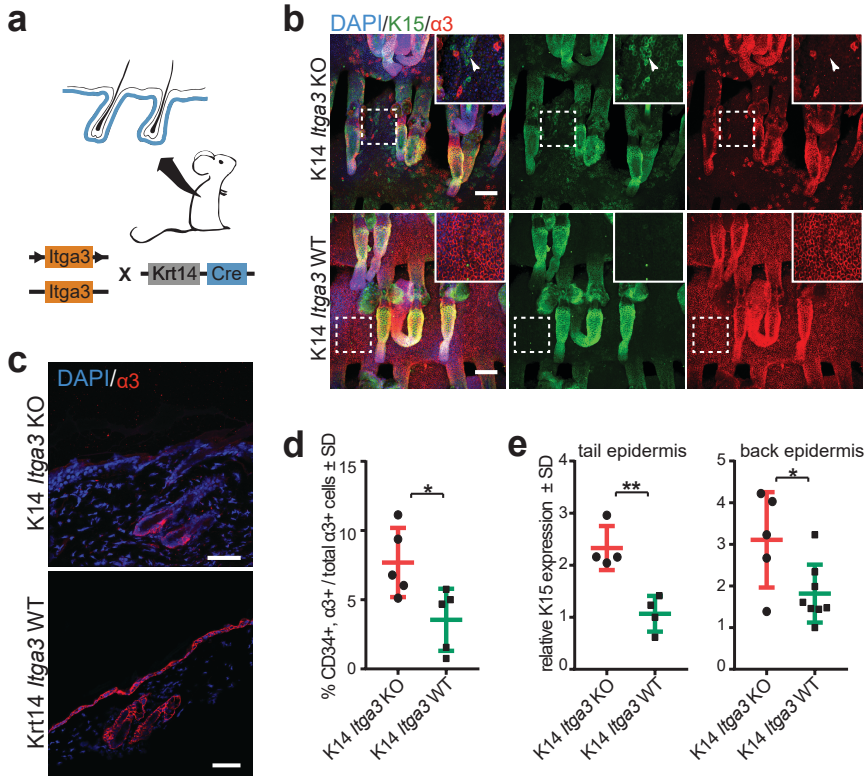

Figure 2: Epidermal deletion of α3β1 causes de novo expression of K15 outside of HBs. (**a**) Overview of the K14 Itga3 KO and WT mouse models. (**b**) Whole mounts of tail epidermis show the presence of α3β1-depleted K15-positive keratinocytes in upper parts of HFs and IFE of K14 Itga3 KO mice (white arrow heads). Remaining α3β1-positive keratinocytes in K14 Itga3 KO mice are preferentially localized to HBs (scale bar: 100 µm). (**c**) Staining for integrin α3 shows HB-localization of α3β1-positive keratinocytes in the back skin of 7-week-old K14 Itga3 KO mice. α3β1 is found in all basal keratinocytes of K14 Itga3 WT mice of similar age (scale bar: 50 µm). (**d**) FACS analysis of keratinocytes isolated from back skin epidermis. The chart shows the percentages of α3-positive HB cells (CD34-positive) in the total α3-positive population. Each dot represents a mouse. Gating strategy can be found in Supplementary figure S2a. (mean ± SD, unpaired t test, *P<0.05). (**e**) GAPDH-normalized relative mRNA expression of K15 is increased in the epidermis of back and tail skin of K14 Itga3 KO compared to WT mice. Each dot represents a mouse and is an average of technical duplicate or triplicate (mean ± SD, unpaired t test, *P<0.05, **P<0.005).

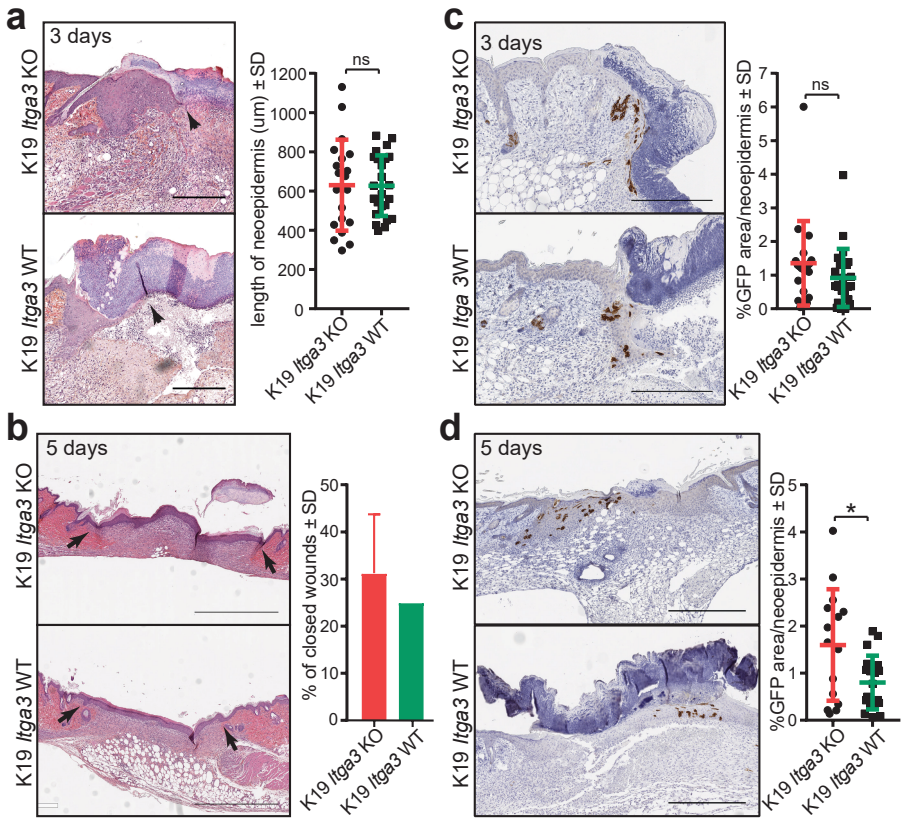

Figure 3: The contribution of HB keratinocytes to newly formed IFE is increased in the absence of α3β1. (**a-b**) H&E staining (left) and quantification (right) of wound-healing. Wound closure is comparable between K19 Itga3 KO and WT mice, 3 (**a**) and 5 days (**b**) after wounding. (**a**) Each dot represents the average length of the neo-epidermis (black arrows) per wound (mean ± SD, unpaired t test). Wounds of 6 K19 Itga3 WT and 5 K19 Itga3 KO mice were analyzed (scale bar: 300 μm). (**b**) Bars represent the percentage of closed wounds per mouse (mean ± SD). Wounds of 4 K19 Itga3 WT and 4 K19 Itga3 KO mice were analyzed (scale bar: 1 mm). (**c-d**) IHC staining for GFP (left) and quantification (right) of GFP-positive area per neo-epidermis of K19 Itga3 KO and WT mice. (**c**) HB-originating GFP-positive keratinocytes comparably contribute to neo-epidermis in K19 Itga3 KO and WT mice 3 days after wounding (scale bar: 300 μm). Each dot represents the percentage of GFP-positive area per wound (mean ± SD, unpaired t test). Wounds of 6 K19 Itga3 WT and 5 K19 Itga3 KO mice were analyzed. (**d**) Five days after the wounding, the contribution of the α3β1-deficient HB SCs to the newly formed epidermis is more extensive than that of the α3β1-proficient HB SCs. Each dot represents the percentage of GFP-positive area per wound (mean ± SD, unpaired t test, *P<0.05). Wounds of 5 K19 Itga3 WT and 4 K19 Itga3 KO mice were analyzed.

By the end of the treatment (P196), ulcerating tumors were observed in one K19 Itga3 KO and three WT mice, which were identified as SCCs (K19 Itga3 KO and WT) and keratoacanthomas with carcinomatous changes (K19 Itga3 WT) by histological analysis (**Supplementary fig. 3b**). As this incidence was too low to draw any conclusions about the role of α3β1 in the malignant progression of tumors, we selected seven K19 Itga3 KO and seven WT mice with low tumor burden and treated them with TPA for up to an additional 10 weeks, until they had to be sacrificed due to the tumor burden or ulceration of tumors. Tumor progression was more commonly observed in K19 Itga3 KO (5 out of 7) compared to K19 Itga3 WT mice (3 out of 7). Furthermore, K19 Itga3 KO mice developed also high malignancy grade tumors such as spindle cell sarcoma and mixed basal SCC in addition to the SCCs and keratoacanthomas with carcinomatous changes (**Supplementary fig. 3c**). Even though the yield of progressed tumors after this prolonged treatment was still too low to draw firm conclusions, the observed trend fits with the results of tumorigenesis experiments previously performed with K14 Itga3 KO and WT mice [14]. All in all, these data show that α3β1 in HB SCs promotes formation of benign tumors during DMBA/TPA treatment.

HB-derived keratinocytes are largely absent from skin tumors

The moderate reduction of tumorigenesis in the K19 Itga3 KO mice, compared to the near complete absence of tumor formation in mice carrying a targeted deletion of Itga3 in the whole epidermis, suggests that HB SCs might be the cells-of-origin for some, but not all DMBA/TPA-initiated tumors. To determine whether papillomas can arise from Cre-initiated HB keratinocytes in K19 Itga3 KO and WT mice, we have analyzed the cross-sectional areas of 321 and 365 tumors, respectively, for the presence of GFP. Remarkably, most tumors were negative for GFP and only one small papilloma isolated from K19 Itga3 WT mouse consisted almost entirely of GFP-positive cells (**Fig. 5a, b**). Consistent with their non-HB origin, all the analyzed tumors stained positive for α3β1 (**Fig. 5c**). 2,8% of tumors, isolated from the K19 Itga3 KO mice and 8,2% of the K19 Itga3 WT tumors contained patches of GFP-positive cells, accounting to up to 5% of the total tumor area (**Fig. 5b**). Such minor cell populations in otherwise monoclonal DMBA/TPA-derived papillomas have been recently described and shown to lack the activating mutation in Hras, the predominant proto-oncogene activated in DMBA/TPA-induced tumors [21]. As the assessment of the amount of HB-originating GFP-positive cells in the tumors was determined based on only one cross section, we reasoned that the actual numbers are likely higher. Indeed, an analysis of 10 cross sections (200 μm step size) in randomly selected tumors of four K19 Itga3 KO and four WT mice showed that respectively, 9,6% and 32,3% of the tumors contain regions of GFP-positive cells. These GFP-positive regions occupy less than 0,1% of the tumor area in the majority of tumors (**Fig. 5d, e**). The number of tumors, containing GFP-positive cells as well as the

GFP-positive regions were significantly reduced in tumors, originating from K19 Itga3 KO, compared to WT mice (**Fig. 5d**). Taken together, these data demonstrate that HB SCs are not the main tumor-initiating cells in the two-stage carcinogenesis model and that HB-derived keratinocytes constitute a minor cell population in some tumors.

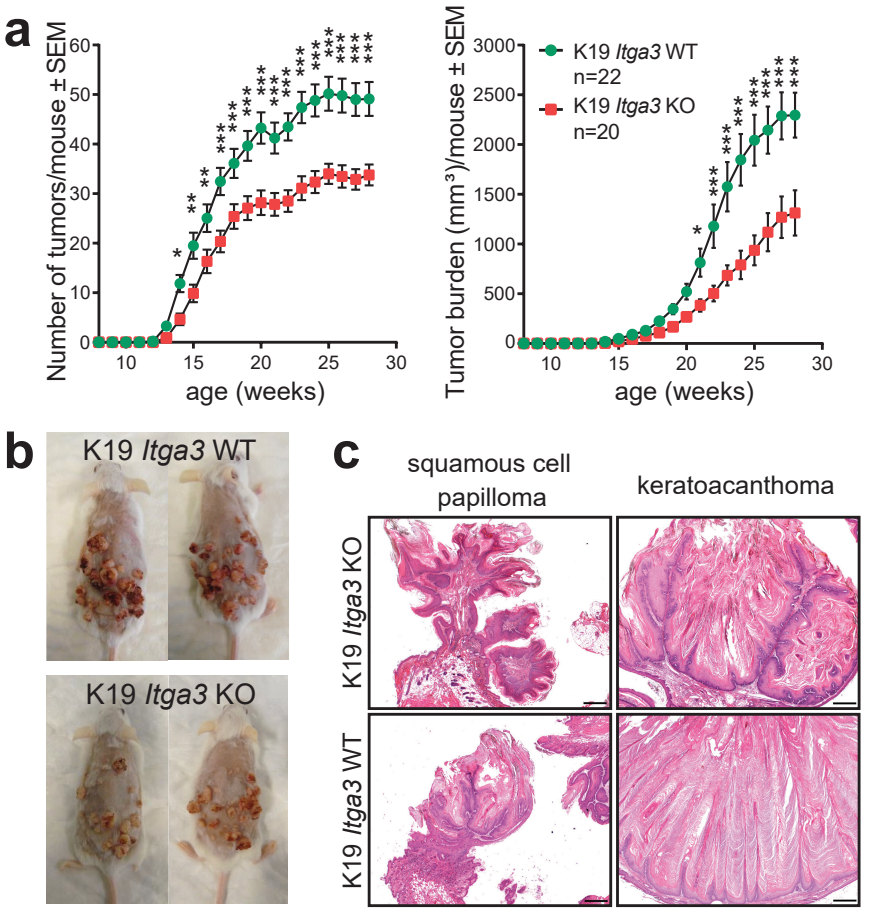

Figure 4: The absence of α3β1 in HBs reduces susceptibility of mice to DMBA/TPA-mediated tumorigenesis. (**a**) The number of tumors (left) and tumor burden (right) is decreased in K19 Itga3 KO compared to WT mice submitted to the DMBA/TPA-carcinogenesis protocol (mean ± SEM, unpaired t test, *P<0.05, **P<0.005, ***P<0.0005). (**b**) Representative macro images of K19 Itga3 KO and WT mice at the end of the treatment. (**c**) Histology of benign papillomas and keratoacanthomas, representing the majority of tumors isolated from K19 Itga3 KO and WT mice.

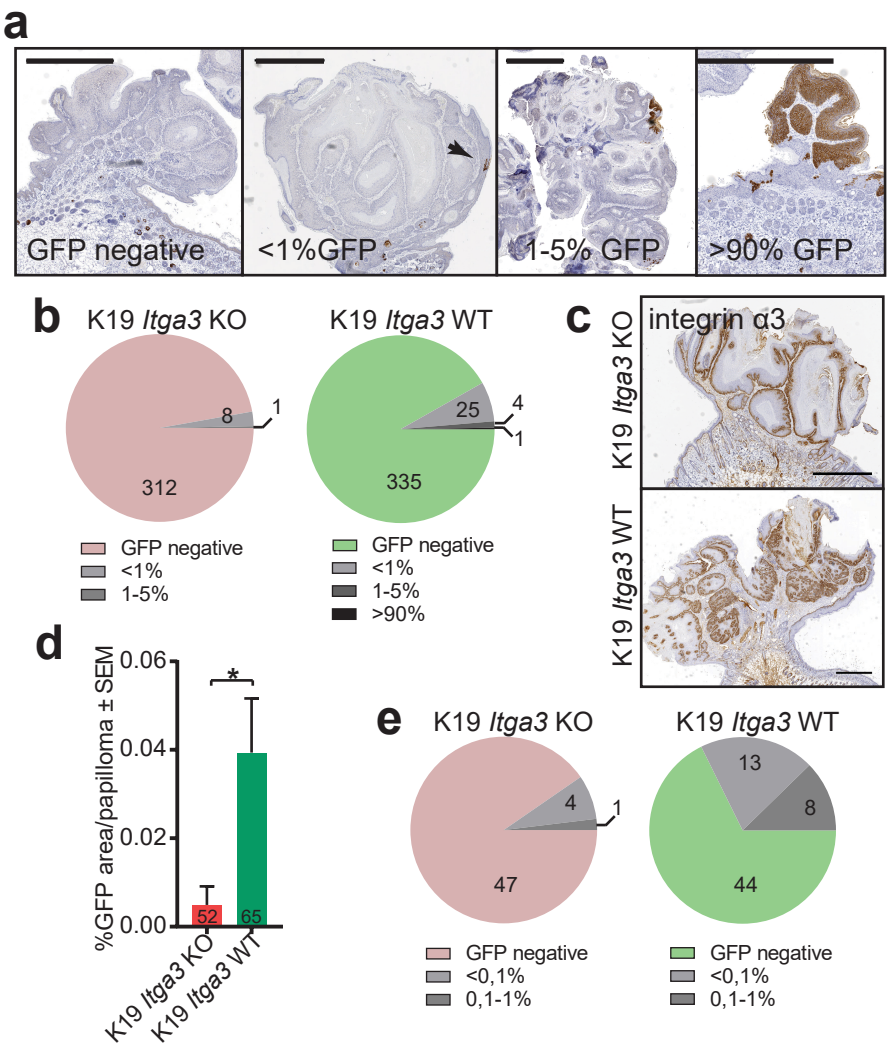

Figure 5: HB-derived keratinocytes are largely absent from skin tumors. (**a-b**) With rare exceptions, Cre-induced GFP-positive cells represent less than 1% of total tumor mass. (**a**) Representative IHC images stained for GFP and (**b**) quantification of GFP-positive area in cross-sections of tumors, isolated from 9 K19 Itga3 KO and 8 WT mice. The vast majority of tumors is GFP-negative (scale bar: 1mm). (**c**) Integrin α3β1 is strongly expressed in all tumors analyzed (scale bar: 1mm). (**d-e**) Analysis of GFP-positive area over 10 cross sections, cut every 200 µm of randomly selected tumors from 4 K19 Itga3 KO and 4 WT mice. (**d**) The contribution of GFP-positive HB-originating keratinocytes to tumors, isolated from K19 Itga3 KO is significantly reduced compared to WT mice (mean ± SEM, unpaired t test, *P<0.05). (**e**) The majority of tumors are GFP-negative in both, K19 Itga3 KO and WT mice. GFP was detected in 9,6% of K19 Itga3 KO and in 32,3% of K19 Itga3 WT tumors and did not exceed 1% of total tumor mass.

α3β1-depleted keratinocytes show an increased differentiation signature and decreased expression of CCN2 during the initiation stage of tumorigenesis

The non-HB origin of the majority of tumors together with the decreased tumorigenesis upon the deletion of HB-derived Itga3 indicate that α3β1 in HB SCs likely promotes tumorigenesis indirectly, i.e. through changes in the pro-tumorigenic environment or by directly affecting neighboring keratinocytes. Because the deletion of Itga3 in HB SCs had a larger effect on the initiation of tumorigenesis than on the rate of tumor growth (**Fig. 4a, Supplementary fig. 3a**), we investigated a potential role of α3β1 in establishing a tumor-supportive environment. To this end, we performed RNA sequencing of GFP-positive keratinocytes isolated from the skin of K19 Itga3 KO and WT mice during the initiation stage of tumorigenesis induced by short-term DMBA/TPA treatment, which has been shown to be sufficient for the outgrowth of papillomas [22,23]. This stage of two-stage chemical carcinogenesis, when pro-tumorigenic pathways are switched on, but tumors have not yet been formed, thus reflects the cell environment that can support tumor formation. At this time point, HB-originating GFP-positive cells can be found in both outer and inner layers of the growing HFs and, interestingly, in some cases in isthmus, infundibulum and IFE of K19 Itga3 KO and WT mice (**Fig. 6a**).

Gene expression profiling of the GFP-positive keratinocytes by RNA-sequencing confirmed their HB origin (e.g. high expression of CD34, Lgr5 and K15) (**Supplementary Fig. 4a**). A total of 15 protein-coding genes were significantly differentially expressed between the GFP-positive Itga3 KO and WT keratinocytes. Several of the hits that displayed an increased expression in Itga3 KO keratinocytes are known to be involved in squamous cell differentiation (**Fig. 6b**), which is in line with previously reported observations of the increased epidermal turnover upon the deletion of Itga3 [14]. Importantly, several of the hits belonged to the keratinocyte secretome, indicating that α3β1 could promote the formation of tumor-permissive environment through regulation of paracrine signaling of the HB SCs (**Fig. 6b**). The high expression of connective tissue growth factor CCN2 (also CTGF) was of particular interest, as this protein has a broad regulatory function in a variety of important biological and pathological processes, is a known integrin interactor and has been implemented in skin tumorigenesis before [24,25]. RNA sequencing data was validated using immunohistochemical and immunofluorescent (IF) staining, which confirmed that CCN2 localizes to HFs and HB SCs of short-term DMBA/TPA-treated back skin (**Fig. 6c, Supplementary Fig. 4b**), as has been previously reported [26,27]. Furthermore, IF staining confirmed the reduction of CCN2 expression in GFP-positive HFs lacking α3β1 (Fig 6c). In papillomas, CCN2 expression could be observed in isolated epithelial or stromal cells and occasionally in cell clusters, which did not correlate to the HB-originating GFP-positive areas in

consecutive sections of tumors, isolated from K19 Itga3 WT mice (**Supplementary fig. 4c, d**). Even though CCN2 could be detected in all K19 Itga3 WT tumors analyzed, a small number of CCN2-positive cells (the mean CCN2-positive surface is 0.27% of total tumor area) together with their non-HB origin indicates that CCN2 does not play a major role in the late stages of tumor growth (**Supplementary fig. 4c**).

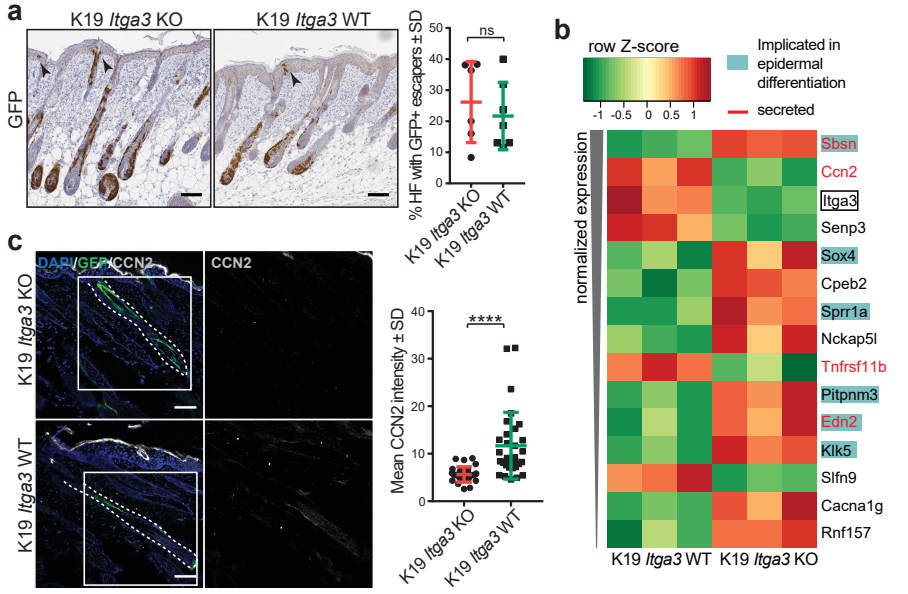

Figure 6: α3β1-depleted keratinocytes show an increased differentiation signature and decreased expression of CCN2 during the initiation stage of tumorigenesis. (**a**) GFP-positive Cre-induced HB SCs localize to growing HFs and, in some cases, to isthmus, infundibulum and IFE (black arrows) after short-term DMBA/TPA treatment in K19 Itga3 KO and WT mice. Left: IHC staining for GFP (scale bar: 100 μm). Right: quantification of the number of HFs, where GFP-positive cells were observed in upper parts of HFs and in adjacent IFE. Each dot represents a mouse (mean ± SD, unpaired t test). (**b**) Heat map of row-scaled significantly differentially expressed protein-coding genes of GFP-positive keratinocytes, isolated from 3 K19 Itga3 KO and 3 K10 Itga3 WT mice after short-term DMBA/TPA treatment. Protein-coding genes have an adjusted P<0.05 and an average normalized expression across all samples >4 (as calculated with Voom) and a logFC>0.6 between K19 Itga3 WT an KO mice. (**c**) IF staining (left) and quantification of mean intensity of the signal (right) for CCN2 in GFP-positive HFs after short-term DMBA/TPA treatment. Each dot represents a GFP-positive HF. HFs of 5 K19 Itga3 KO and 6 K19 Itga3 WT mice were quantified (mean ± SD, unpaired t test, P<0.0001).

Together, this data shows that during the initiation stage of tumorigenesis α3β1 in HB SCs suppresses HF differentiation and regulates the expression of CCN2 and several other proteins that are part of HB SC secretome. Thus, α3β1 might affect

the cell environment during early tumorigenesis through regulation of the paracrine signaling.

CCN2 expression is α3β1-dependent and promotes colony formation and 3D growth of *Hras* transformed keratinocytes *in vitro*

Next, we investigated whether α3β1 regulates the expression of CCN2 in Hras transformed keratinocytes, isolated from K14 Itga3 WT mice that underwent the full DMBA/TPA carcinogenesis protocol (MSCC WT and MSCC Itga3 KO keratinocytes) [14]. In agreement with our observations in mice, deletion of α3β1 in MSCC keratinocytes resulted in reduced levels of CCN2 mRNA (**Fig. 7a**). Furthermore, MSCC WT keratinocytes showed an increased expression of CCN2 when the conditions that occur during DMBA/TPA treatment were mimicked by application of either TPA or IL-6, the cytokine upregulated during DMBA/TPA tumorigenesis and crucial for tumor formation [28] (**Fig. 7a**). Integrin α3β1-dependent expression of CCN2 and its increase upon TPA and IL-6 treatment were confirmed at the protein level using IF and western blot analysis (**Fig. 7b, c, Supplementary fig. 5a**). Furthermore, IF analysis showed that MSCC WT keratinocytes secrete CCN2, which colocalized with deposited laminin-332 (**Fig. 7b, Supplementary fig. 5b**).

To assess whether CCN2 contributes to the tumorigenic properties of transformed keratinocytes in vitro, we generated two CCN2 KO clones using CRISPR/Cas9 with two distinct guide RNAs (MSCC CCN2 KO G1 and MSCC CCN2 KO G2) (**Fig. 8a**) and submitted them to colony formation assay. In line with observations in K14 Itga3 KO mice, the deletion of α3β1 resulted in a strong reduction of colony formation and in decreased colony size (**Fig. 8b and Supplementary fig. 6a**). Even though the deletion of CCN2 did not influence colony size, the colony-forming ability of the two CCN2 KO clones was significantly reduced compared to WT MSCC and control clones (**Fig. 8b and Supplementary fig. 6a**). Next, we tested whether secreted CCN2 can promote survival of transformed keratinocytes by treating Itga3 KO MSCCs and CCN2 KO clones with exogenous CCN2. CCN2 treatment significantly increased the colony formation of CCN2 KO MSCCs, albeit not to the level of the MSCC control clones (**Fig. 8c, Supplementary fig. 6b**). No differences in colony formation could be observed upon the treatment of Itga3 KO MSCCs with CCN2 (**Fig. 8d, Supplementary fig. 6b**), indicating that α3β1-mediated secretion of CCN2 may enhance the tumorigenic potential of keratinocytes, but is not sufficient for tumorigenesis. We further investigated whether α3β1 and CCN2 affect the three-dimensional (3D) growth of MSCC keratinocytes using Matrigel matrix. The results showed that at the beginning of spheroid formation, CCN2 expression was dependent on integrin α3β1 (**Fig. 8e**). Furthermore, spheroids needed α3β1 to successfully accumulate mass in the 3D matrix (Fig 8e, f). Importantly, even though

CCN2 KO clones still formed 3D spheroids, their size was significantly reduced compared to CCN2 control clones and MSCC WT keratinocytes (**Fig. 8f**). In 3D culture, seeding the CCN2 KO MSCC clones in the presence of two different concentrations of CCN2 slightly increased their growth potential (**Fig. 8g, Supplementary fig. 6c**), which was not observed when CCN2 MSCC cells were treated three days after seeding, when spheroids had already been formed **(Supplementary fig. 6d**).

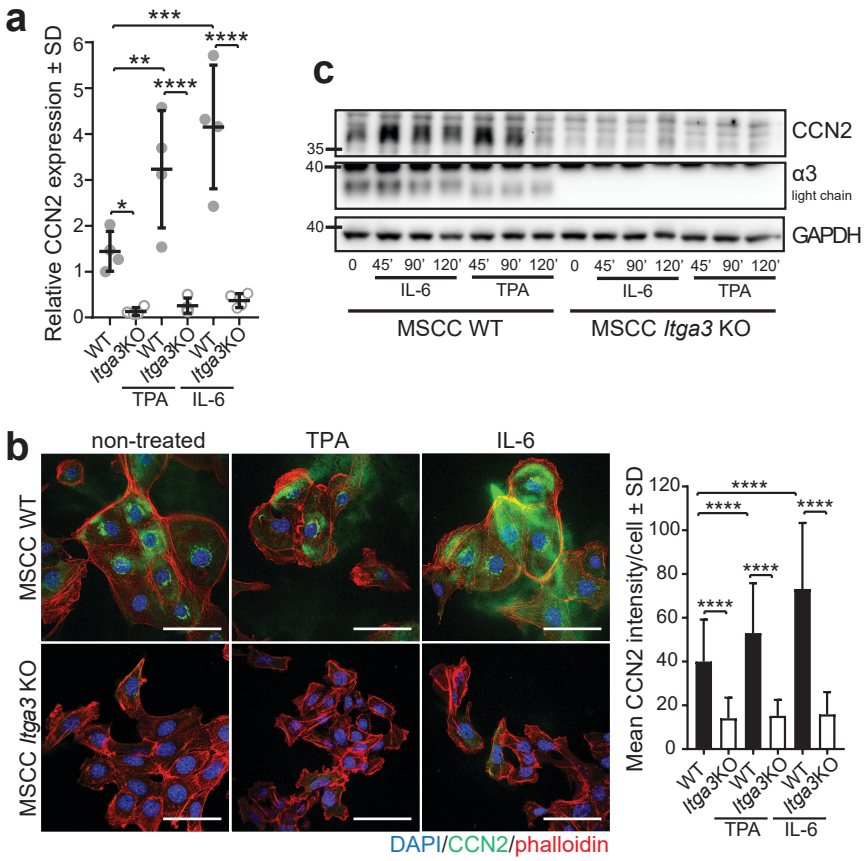

Figure 7: CCN2 expression in transformed keratinocytes is α3β1-dependent. (**a**) GAPDH-normalized relative mRNA expression of CCN2 is significantly decreased in non-stimulated as well as IL-6 and TPA-treated α3β1-depleted keratinocytes. The average of up to four independent measurements of technical duplicates of 4 independent samples is presented (mean ± SD, Fisher's LSD test, *P<0.05, **P<0.005, ***P<0.0005, ****P<0.0001). (**b**) IF (left) and quantification of the mean intensity (right) of CCN2 in non-stimulated, IL-6 and TPA-treated MSCC Itga3 KO and WT keratinocytes. Expression of CCN2 is α3β1-dependent and increases upon IL-6 and TPA treatment (scale bar: 50 μm). 90 cells imaged over 3 independent experiments were quantified (mean ± SD, Fisher's LSD test, P<0.0001). (**c**) Representative WB confirming α3β1-dependent and IL-6 and TPA-mediated CCN2 expression. Quantification can be found in Supplementary figure S5a.

This is in agreement with our previous observations of low CCN2 expression during late stages of tumor and spheroid growth (**Fig. 8e, Supplementary fig. 4c**) and could further indicate that exogenous CCN2 may enhance tumorigenic potential of transformed keratinocytes during early stages of tumorigenesis, however in later stages it likely does not play a major role. However, as CCN2 can associate with extracellular matrix components [25], which we observed also in this study (**Supplementary fig. 5b**), it is conceivable that the concentration of CCN2 that reached cells within the inner layers of spheroids was too low to promote the growth of already formed spheroids, despite the high concentration of CCN2 used (**Supplementary fig. 6d**). Finally, we confirmed that α3β1-expression is an essential prerequisite for CCN2-mediated promotion of tumorigenesis, as seeding Itga3 KO MSCC with CCN2 had no effect on their 3D growth (**Fig. 8h**).

Together, this data shows that CCN2 plays a role in supporting the tumorigenic potential of α3β1-expressing transformed keratinocytes in vitro, which makes it a likely player in our in vivo tumorigenesis mouse model.

DISCUSSION

The previous hypothesis on the mechanism behind the essential role of integrin α3β1 in DMBA/TPA-induced tumorigenesis heavily weighted on the idea that HB SCs represent the cancer cells-of-origin and that the deletion of α3β1 promotes their egress into IFE [14]. Here, we show that the deletion of α3β1 in HB keratinocytes causes a slight increase in their egress only during wound-healing. As the egress of HB SCs and α3β1-mediated suppression of keratinocyte migration during wound-healing is well established, such role of HB-residing α3β1 in wound re-epithelization is not unexpected [4,20,29]. More surprising is the observation that the deletion of α3β1 does not cause the egress of HB SCs under normal homeostatic conditions, even though α3β1-depleted, K15-positive keratinocytes are found in the upper parts of HF and in IFE of K14 Itga3 KO mice [14]. As the deletion of α3β1 causes an increased epidermal turnover in K14 Itga3 KO mice [14], our finding that these keratinocytes express K15 de novo ties well with the reported close relationship between K15 expression and the loss of homeostasis of the epidermal differentiation program in basal-like cells [17].

The DMBA/TPA-induced skin carcinogenesis model mimics the multi-stage nature of cancer, in which substantial time is needed for tumors to outgrow from cancer-initiating cells. In line with this, the importance of slow-cycling, label-retaining cells in DMBA/TPA-initiated tumorigenesis has long been established [30,31].

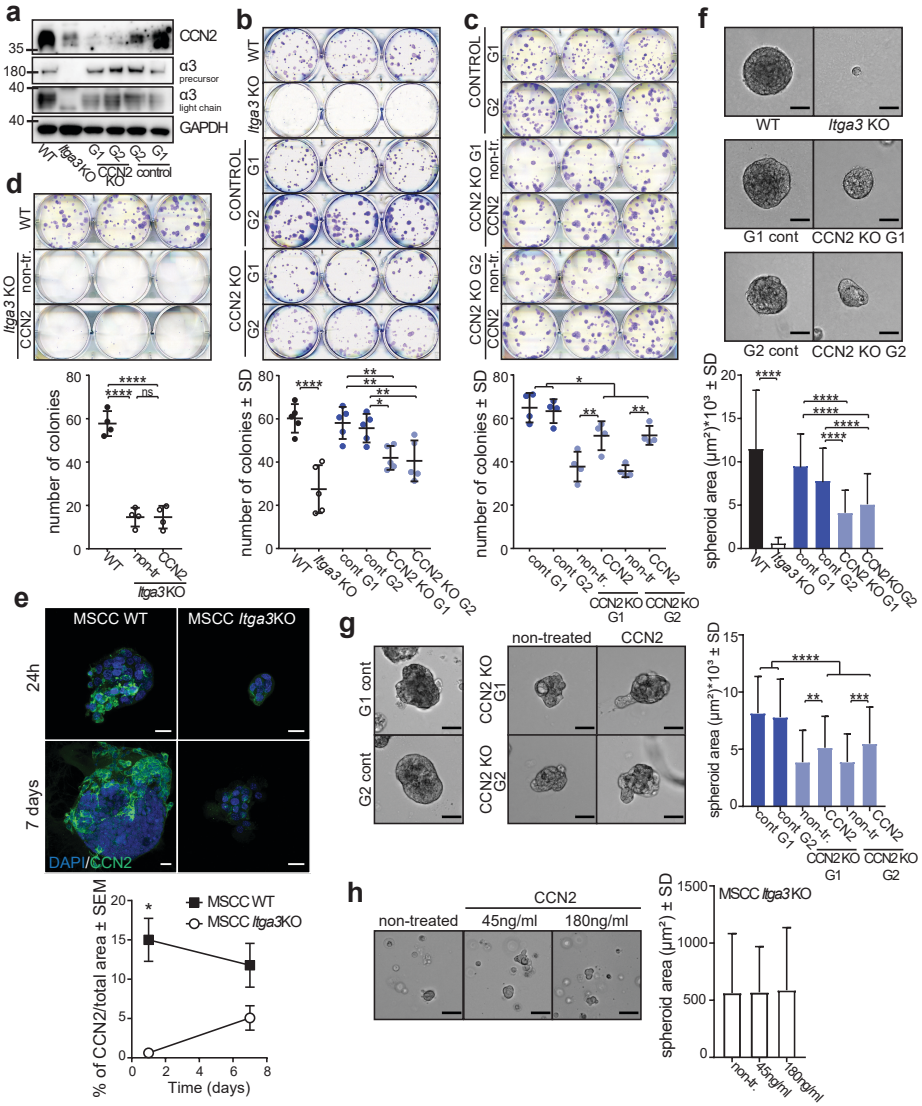

Figure 8: CCN2 promotes colony formation and 3D growth of transformed keratinocytes expressing α3β1. (**a**) WB of CCN2 and integrin α3-expression of selected CCN2 KO and control clones. (**b**) Representative image (top) and quantification (bottom) of colony formation assay of MSCC Itga3 WT and Itga3 KO cells and MSCC CCN2 KO G1, KO G2, control G1 and control G2 clones. Deletion of α3β1 results in a strong reduction of colony formation and colony size. Moderate reduction of colony formation can be seen upon CCN2 deletion. Quantification of colony size can be found in Supplementary figure S6a. Average values of technical triplicates of 5 independent experiments are presented (mean ± SD, Fisher's LSD test, *P<0.05, **P<0.005, ****P<0.0001). (**c**) Representative image (top) and quantification (bottom) of colony formation assay of MSCC CCN2 KO G1 and KO G2 clones, grown in control conditions or in the presence of 45 ng/ml CCN2, as well as CCN2 WT control G1 and

control G2 clones. Treatment with exogenous CCN2 significantly increases colony formation of CCN2 KO clones. Quantification of colony size can be found in Supplementary figure S6b. Average values of technical triplicates of 4 independent experiments are presented (mean ± SD, Fisher's LSD test, *P<0.05, **P<0.005). (**d**) No differences in the number of colonies can be observed upon CCN2 treatment of Itga3 KO transformed keratinocytes. Quantification of colony size can be found in Supplementary figure S6b. Average values of technical triplicates of 4 independent experiments are presented (mean ± SD, Fisher's LSD test, ****P<0.0001). (**e**) Quantification (left) and IF as maximum intensity projection (right) of CCN2 expression of MSCC Itga3 WT and KO spheroids, grown in 3D Matrigel matrix for 1 or 7 days (scale bar: 20 μm). The expression of CCN2 is α3β1-dependent, which is particularly prominent at the beginning of spheroid growth. The percentage of CCN2-positive area was quantified from 17 MSCC Itga3 KO and 30 MSCC Itga3 WT spheroids 1 day after seeding and from 15 MSCC Itga3 KO and 27 MSSC WT spheroids 7 days after seeding (mean ± SEM, unpaired t test, *P<0.05). (**f**) Spheroid growth in 3D Matrigel is α3β1-dependent and moderately reduced upon CCN2 deletion. Top: bright filed images of representative spheroids (scale bar: 50 μm). Bottom: size quantification of 60-80 spheroids measured over 3 to 4 independent experiments (mean ± SD, Fisher's LSD test, ****P<0.0001). (**g**) 3D growth of CCN2 KO MSCC spheroids shows small but significant increase when cells are seeded with 45 ng/ml of CCN2. Left: bright filed images of representative spheroids (scale bar: 50 μm). Right: size quantification of 85-90 spheroids measured over 3 independent experiments (mean ± SD, Fisher's LSD test, **P<0.005, ***P<0.0005 ****P<0.0001). (**h**) Seeding Itga3 KO MSCCs with 45 ng/ml or 180 ng/ml of CCN2 does not impact 3D growth pf spheroids. Left: bright filed images of representative spheroids (scale bar: 50 μm). Right: size quantification of 70 spheroids measured over 2 independent experiments (mean ± SD, One-way ANOVA P=0.9491).

Therefore, a loss of initiated label-retaining stem cells due to their premature terminal differentiation during increased epidermal turnover remains a plausible cause of the near complete absence of tumorigenesis in K14 Itga3 KO mice [14]. The finding that α3β1 affects epidermal turnover was confirmed in this study, where we an increased differentiation gene signature in GFP-positive cells, isolated from K19 Itga3 KO mice, although the differences in differentiation were not substantial enough to affect the hair cycle or hair growth in mice. This was expected, as hair cycle was not altered in K14 Itga3 KO mice of similar age [14], although the loss of integrin α3β1 has been shown to affect hair follicle maintenance and morphology in mice, bred onto C57Bl/6 background [14,32].

HB SCs have often been suggested to be the main cells-of-origin for DMBA/TPA-initiated tumors [33–36]. However, several studies have demonstrated that other epidermal cell populations can also act as cancer SCs in the DMBA/TPA model of skin carcinogenesis [9,15,16,30]. Considering also the fact that the K15 promoter, which is commonly used for HB-specific genetic modifications, does not target this compartment exclusively [9], there is an emerging consensus that several epidermal SC populations can serve as cells-of-origin for DMBA/TPA-initiated tumors, albeit that there are likely differences in their fate during the progression of the disease [11,30]. In this study, we showed that the contribution of HB SCs to skin tumors is minimal, and even further reduced in the K19 Itga3 KO mice. A similar observation was made by Goldstein and co-workers, when

they used the K19 promoter to target the deletion of the transcription factor Nfatc1 in HBs [37]. A recent, thorough study by Reeves et al. (2018) demonstrated that DMBA/TPA treatment induces papillomas that are mostly monoclonal but often contain additional minor populations at the edges of tumors. Interestingly, these minority populations, which resemble our HB-originating tumor patches, commonly do not possess driver Hras mutation and in carry a lower mutational load [21].

Despite their near absence in skin tumors, HB SCs affected tumor incidence and, to a much lesser degree, tumor size in an α3β1-dependent manner. The possibility that HB SCs can affect (rather than be) cancer-initiating cells has received undeservedly little attention. Only a very recent study by the research group of Valentina Greco demonstrated that HB SCs exhibit tolerance to Hras mutation and non-autonomously affect neighboring epithelial and stromal cells [38]. Our observations of HB-originating GFP-positive cells in IFE and upper parts of HFs during initiation of tumorigenesis indicate that α3β1 could affect neighboring cells and/or promote a permissive tumor environment in different epidermal niches. Furthermore, small HB-derived cell populations in tumors may also affect the survival and/or proliferation of neighboring tumor cells.

It is well established that the cellular environment, composed of fibroblasts, endothelial cells, and immune cells, plays a crucial role in development and progression of DMBA/TPA-initiated tumors [33,39–41]. Over the past few years, the role of integrins beyond adhesion and biomechanical transduction of signals has become more evident, especially in their ability to modulate the tumor microenvironment [42]. In particular, integrin α3β1 has been shown to regulate paracrine signaling and crosstalk between cells, among others by controlling the expression of secreted cellular proteins [43–45]. This is in line with our findings that the expression of CCN2 in HB keratinocytes in vivo and in mouse keratinocytes in vitro depends on α3β1. CCN2 has been implemented in skin tumorigenesis previously and is an interesting potential player in DMBA/TPA-induced skin cancer because its expression can be regulated by several proteins, essential for tumor formation in this model, such as FAK, YAP, TGFβ and Stat3 [8,24,25,46–48]. Moreover, it can directly interact with integrins, as well as with cytokines, such as TGFβ, and heparan sulfate proteoglycans, which are abundantly present in the basement membrane of the skin, and thus can modulate related signal transduction pathways and their crosstalk [25]. Furthermore, it was shown that the expression of CCN2 in mesenchymal cells in the skin and lungs affects a differentiation program of adjacent epithelial cells [49], which fits well with the role of α3β1 in the DMBA/TPA tumorigenesis model. As the expression of CCN2 in full-grown papillomas is very low and could not be correlated to HB-originating areas by histochemistry, its potential pro-tumorigenic

role likely occurs during the initiation stage of DMBA/TPA-driven tumorigenesis. This is supported by our in vitro studies, where CCN2 increased the clonogenic potential and initiation of 3D growth of transformed keratinocytes. However, it is clear that these in vitro studies cannot be used for drawing definitive conclusions concerning the role of CCN2 in vivo, and that further work is needed to explore this role. It would be particularly interesting to see if the deletion of CCN2 in HBs reduces the formation of papillomas in mice subjected to the two-stage carcinogenesis protocol.

It is important to note that the effect of CCN2 deletion on the *in vitro* tumorigenic properties of transformed keratinocytes is weak to moderate compared to the pronounced effect of the deletion of Itga3. Furthermore, the ability of CCN2 to promote the survival and outgrowth of transformed keratinocytes depends on the expression of α3β1. Thus, CCN2 may enhance tumorigenesis but is not essential for it. Considering also the fact that the deletion of α3β1 in HB SCs fails to completely recapitulate the effect of total epidermal α3β1 deletion on tumorigenesis, there must be additional α3β1-dependent functions that are relevant to tumor initiation and formation. Therefore, our study reopens the question of the mechanism behind the essential role of α3β1 in DMBA/TPA-driven tumorigenesis. Here, we disprove the original hypothesis that the dramatic effect of epidermal α3 deletion can be explained by the egress of HB SCs. Furthermore, we show that α3β1 in HB SCs contributes to tumorigenesis, however its moderate effect strongly indicates that there are additional mechanisms in play, which will have to be re-examined.

Even though K19 promoter targets the HB with high specificity, a limitation of the K19-CreER mouse model is the low efficiency of Cre-mediated recombination. We have observed Cre-induction in majority of HFs, however α3β1 has not been deleted in all the HBs, which could mean that the contribution of HB-originating cells to tumor mass has been understated. With this concern in mind we have analyzed a large number of tumors for HB-originating, GFP-positive cells. As we found only 1 tumor out of 365 to consist entirely of GFP-positive cells, we believe that the conclusion that HB SCs do not represent the main cancer cell-of-origin is credible. The remaining α3β1-positive cells in HBs of K19 Itga3 KO mice could also lead to skewed effects of the deletion of α3β1 in HBs in tumorigenesis assays. This is of lesser concern, as we observed non-efficient deletion of α3 also in the HBs of K14 Itga3 KO mice, i.e. the model in which DMBA/TPA-treatment resulted in near absence of tumor formation. Furthermore, it should be noted that differences between the two models may arise because of the different timing of Itga3 deletion in the K14 Itga3 KO and K19 Itga3 KO mice. However, the subtility of the phenotype of constitutive Itga3 epidermal deletion at the age when HB-specific Itga3 deletion was induced in K19-driven mouse model offers some reassurance that

our findings with the K19 Itga3 KO mice can be related to those with the K14 Itga3 KO mice [20].

In conclusion, we show that α3β1 in HB SC population indirectly contributes to skin tumorigenesis. Integrin α3β1-regulated expression of matricellular protein CCN2 during the initiation of tumorigenesis indicates that α3β1 might mediate paracrine signaling and thus promote the formation of a permissive tumor environment. The role of CCN2 as a potential player in α3β1-mediated tumorigenesis was demonstrated in transformed keratinocytes in vitro. Even though our findings elucidate only parts of the mechanism underlying the essential function of α3β1 in DMBA/TPA-driven tumorigenesis, they provide a new understanding of the role of HB SCs in skin tumorigenesis as well as offer an important insight into complex and diverse ways in which integrins can affect this disease.

MATERIALS AND METHODS

Generation of mice

K19-CreER mice [18] were intercrossed with mT/mG mice (Gt(ROSA)26Sortm4(ACTB-tdTomato,-EGFP)Luo , Jackson Laboratory strain 007576) to obtain K19-CreER; mT/mG mice (K19 Itga3 WT mice). K19-CreER; mT/mG mice were further intercrossed with Itga3fl/fl (i.e. Itga3tm1Son/tm1Son according to Mouse Genome Informatics) to obtain K19-CreER; mT/mG; Itga3fl/fl (K19 Itga3 KO) mice. Epidermis-specific mice are named Krt14tm1(cre)Wbm (K14 Itga3 WT mice) and Krt14tm1(cre)Wbm; Itga3tm1Son/tm1Son (K14 Itga3 KO mice) according to the Mouse genome Informatics and have been described before [14]. All mice were bred onto an FVB/N background. All animal studies were performed according to Dutch guidelines for care and use of laboratory animals and were approved by the animal welfare committee of the Netherlands Cancer Institute.

Animal experiments

A DMBA/TPA-carcinogenesis protocol has been previously described [14]. Briefly, backs of 6-week old mice were shaved and after a week topically treated with 30μg (in 200μl acetone) of DMBA (Sigma, D3254), followed by bi-weekly topical applications of 12,34μg (in 200μl acetone) of TPA (Sigma, P1585) for 20 weeks. A similar procedure was used for short-term DMBA/TPA treatment; however, mice were only treated with four doses of TPA over two weeks following DMBA treatment. To induce Cre-recombinase, 5-week and 5-day old mice were injected intraperitoneally (IP) for four days with 2,5 mg/ml of tamoxifen (Sigma, T5648) dissolved in sunflower oil per day and (at 6 weeks) additionally topically treated with two doses of 200 μl of 20 mg/ml of tamoxifen dissolved in ethanol.

For linage tracing, 3-week old mice were given an intraperitoneal injection of 2,5 mg/ml of tamoxifen dissolved in sunflower oil per day for four consecutive days. After indicated time points, mice were killed, and the skin was isolated and processed for immunofluorescence, immunohistochemistry or flow cytometry analysis, and/or for RNA isolation. Wound-healing experiments were performed as described previously [50]. 5-week and 5-day old mice were given an intraperitoneal injection of 2,5 mg/ml of tamoxifen dissolved in sunflower oil per day for four consecutive days. 7-week old mice were anesthetized and shaved, and four full-thickness excision wounds of 4mm diameter were cut with small scissors (2 per either side of the dorsal midline). Complete wounds including surrounding tissue were excised 3 and 5 days after injury. Paraffin sections across the middle of the wounds were used for histological analysis of the wound closure. 10 consecutive sections cut every 100µm were used for quantification of the GFP-positive area per area of neo-epidermis.

Immunohistochemistry

Skin, tumors and tails were isolated, fixed in ethanolglacial acetic acid mixture (3:1), containing 2% of formaldehyde (EAF) and/or formaldehyde, embedded in paraffin, sectioned and stained for hematoxylin and eosin (H&E) and/or immunohistochemistry (see table 1). Images were taken with PL APO objectives (10×/0.25 NA, 40×/0.95 NA, and 63×/1.4 NA oil) on an Axiovert S100/AxioCam HR color system using AxioVision 4 software (Carl Zeiss MicroImaging) or with the Aperio ScanScope (Aperio, Vista, CA, USA), using ImageScope software version 12.0.0 (Aperio). Tumor classification was performed blindly. Image analysis was performed using ImageJ [51,52].

Immunofluorescence and whole mounts

Skin was isolated and embedded in Tissue-Tek OCT (optimal cutting temperature) cryoprotectant. Cryosections of skin were prepared, fixed in ice-cold acetone, and blocked with 2% bovine serum albumin (BSA, Sigma) in PBS for 1h at room temperature. Whole mounts of tail epidermis were isolated as described previously [14], fixed in 4% paraformaldehyde in PBS and permeabilized and blocked in PB buffer (20 mM Hepes buffer, pH 7.2, containing 0.5% (vol/vol) TrotonX-100, 0.5% (wt/vol) skim milk powder, and 0.25% (vol/vol) fish skin gelatin). MSCC cells were fixed with 2% paraformaldehyde for 10 min, permeabilized with 0.2% Triton-X-100 for 5 min, and blocked with PBS containing 2% BSA for 1h at room temperature. Spheroids were retrieved from Matrigel by incubation with Cell recovery solution (CorningTM, 354253) for 1h at 4°C and subsequently resuspended in ice-cold PBS. Isolated spheroids were mounted on Poly-L-Lysine (Santa Cruz, 25988-63-0)-coated slides, fixed in 4% paraformaldehyde in PBS for 10 min, permeabilized with 0.2% Triton-X-100 for 5 min, and blocked with PBS containing 2% BSA for 1 h at room temperature. Tissues, spheroids and cells

were incubated with the indicated primary antibodies (see Table 1) in 2% BSA in PBS (whole mounts: PB buffer) for 60 min (whole mounts and spheroids: overnight), followed by incubation with secondary antibodies diluted 1:200 for 60 min (whole mounts: overnight). All samples where counterstained with DAPI for 5 min at room temperature and, when indicated, filamentous actin was visualized using Alexa Fluor 488-conjugated phalloidin (Invitrogen). Cryosections were mounted in Vectashield (Vector Laboratories H-1000) and other samples in Mowiol. Samples were analyzed by Leica TCS SP5 confocal microscope with a 10 or 20x (NA 1.4) objective or 40 and 63x (NA 1.4) oil objective and processed using ImageJ [51,52].

Flow cytometry

Keratinocytes were isolated from mouse back skin as described before [53], washed in PBS containing 2% FCS, and incubated for 1 h at 4°C in primary antibody (see table 1) in PBS 2% FCS. In case of non-fluorophore conjugated antibodies, cells were subsequently incubated with donkey anti-goat Alexa Fluor 647 (Invitrogen; 1:200 dilution) antibody for 30 min at 4°C. Cells were analyzed on a Becton Dickinson FACS Calibur analyzer after the addition of indicated life/dead cell marker. For fluorescent activated cell sorting, GFP-positive cell population was obtained using a Becton Dickinson FACSAria IIu cell sorter.

RT-qPCR

Keratinocytes were isolated from mouse back skin as described before [50], pelleted by centrifugation and resuspended in Trizol reagent (Invitrogen, 15596018). Whole mounts of tail epidermis were isolated [14] and homogenized in Trizol reagent using Polytron, while keeping the temperature of the tissue at 4°C. 10cm dishes of semi-confluent cells were washed with cold PBS, scraped and collected in 2 ml of Trizol reagent. Total RNA was extracted according to the manufacturer's recommendations (Trizol reagent) and 3µg of purified RNA was used to synthesize the first-strand cDNA using First strand cDNA synthesis kit (Thermo scientific, K1612). Quantitative PCR analyses were performed using a Sybr Green gPCR Master mix (Thermo scientific, K0251) and ABI Prism 7500 Real Time PCR System (Applied Biosystems) real-time PCR system. Analysis of results was performed with 7500 Fast System SDS software v 1.4 (Applied Biosystems). Results were presented as relative quantification (RQ) of the ratio of K15 or CCN2 Ct over the GAPDH Ct. Following primers were used 5'-TGAGAAGGTGACCATGCAGA-3' and 5'-GGCAGCCAGAATCGGATCTC-3' for keratin 15, 5'-AGAACTGTGTACGGAGCGTG-3' and 5'-GTGCACCATCTTTGGCAGTG-3' for CCN2 and 5'-ACTCCACTCACGGCAAATTC-3' and 5'-TCTCCATGGTGGTGAAGA-3' for GAPDH.

Expression analysis of HB-originating keratinocytes

Keratinocytes from back skin of short-term DMBA/TPA-treated mice were isolated as described before and FACS-sorted for GFP-positive cells. The total RNA from was isolated using the RNeasy Mini Kit (74106, Qiagen), including an on-column DNase digestion (79254, Qiagen), according to the manufacturer's instructions. Quality and quantity of the total RNA was assessed by the 2100 Bioanalyzer using a Nano chip (Agilent, Santa Clara, CA). Total RNA samples having RIN>8 were subjected to library generation. Strand-specific libraries were generated using the TruSeq Stranded mRNA sample preparation kit (Illumina Inc., San Diego, RS-122-2101/2) according to the manufacturer's instructions (Illumina, Part # 15031047 Rev. E). Briefly, polyadenylated RNA from intact total RNA was purified using oligo-dT beads. Following purification, the RNA was fragmented, random primed and reverse transcribed using SuperScript II Reverse Transcriptase (Invitrogen, part # 18064-014) with the addition of Actinomycin D. Second strand synthesis was performed using Polymerase I and RNaseH with replacement of dTTP for dUTP. The generated cDNA fragments were 3' end adenylated and ligated to Illumina Paired-end sequencing adapters and subsequently amplified by 12 cycles of PCR. The libraries were analyzed on a 2100 Bioanalyzer using a 7500 chip (Agilent, Santa Clara, CA), diluted and pooled equimolar into a multiplex sequencing pool. The libraries were sequenced with 65 base single reads on a HiSeq2500 using V4 chemistry (Illumina Inc., San Diego). Demultiplexing of the reads was performed with Illumina's bcl2fastq. Demultiplexed reads were aligned against the mouse reference genome (build 38) using TopHat (version 2.1.0, bowtie 1.1). TopHat was supplied with a known set of gene models (Gene Transfer Format file (GTF) Ensembl version 77) and was guided to use the first-strand as the library-type. As additional parameters --prefilter-multihits and --no coverage were used. In order to count the number of reads per gene, a custom script which is based on the same ideas as HTSeq-count has been used. For each sample, uniquely mapped sequencing reads were used in order to get the genecounts for all genes present in the GTF file. The strandedness of the mapped reads was taken into account. Differentially expressed analysis was performed using the R packages Limma/EdgeR. Reads that have zero counts across all samples were removed from the dataset. Samples were normalized to counts per million using the 'Voom' function from the Limma package. Gene expressions used for visualization purposes are normalized to 10 million reads and log2 transformed. Before log2 transformation, 1 pseudocount was added in order to avoid negative gene expressions.

Cell culture

MSCC WT and Itga3 KO cells were generated as described [14] and cultured in DMEM with 10% heat-inactivated FCS and antibiotics at 37°C in a humidified, 5% CO2 atmosphere. For CRISPR/Cas9-mediated CCN2 deletion, we cloned target sgRNAs against CCN2 (exon

2; guide1: 5'-ACTCCGATCTTGCGGTTGGC-3'; guide2: 5'-CTCCGATCTTGCGGTTGGCG-3') into pX330.pgkpur vector (a kind gift from the lab of Hein te Riele [54]). MSCC WT cells were transiently transfected with this vector using lipofectamine® 2000 (Invitrogen). Cells were selected with 5 µg/ml of puromycin and puromycin-resistant bulk population was single-cell cloned. Clones were analyzed for the expression of CCN2 using WB analysis. For IL-6 and TPA stimulation of MSCC we added 10 ng/ml of recombinant human IL-6 (R&D Systems, 206-IL) or 100 ng/ml of TPA to DMEM 10% FCS and incubated cells with the mixture for 45 min (for IF and RT-qPCR analysis) or for 45, 90 and 120 min (for WB analysis). For 3D cell culture, 70 µl of growth factor reduced Matrigel Basement Membrane Matrix (Corning, 354230) was pipetted per well of chilled 96-well plate and incubated for 30 min at 37°C. 1000 cells in cold DMEM containing 10% FCS and 2% Matrigel were seeded on top of Matrigel layer and grown for up to 7 days. For CCN2-treatment experiments, cells were seeded in the presence of 45 ng/ml or 180 ng/ml of mouse recombinant CCN2 (Biovendor, RD272589025) and cultured for up to 9 days. Where indicated, 180 ng/ml of CCN2 was added to growth medium of non-treated spheroids on day 3. Medium and CCN2 was refreshed every 3 days of 3D cell culture.

Colony formation assay

Hundred cells in DMEM 10 % FCS were seeded per well of a 6-well plate and incubated at 37°C in a humidified, 5% CO2 atmosphere for 6 days. Where indicated, 45 ng/ml of CCN2 was added to cells during seeding. Colonies were fixed in chilled methanol for 20 min, washed with PBS and stained with crystal violet. Stained plates were scanned and colony number and size was quantified using ImageJ [51,52].

Western Blot

Protein lysates were obtained from sub-confluent cell cultures by lysis in RIPA buffer (20 mM Tris-HCl (pH 7.5), 100 mM NaCl, 4 mM EDTA (pH 7.5), 1% Nonidet P-40, 0.1% SDS, 0.5% sodium deoxycholate) supplemented with 1.5 mM Na_3VO_4, 15 mM NaF (Cell Signaling) and protease inhibitor cocktail (Sigma). Lysates were cleared by centrifugation at 14.000 x g for 20 min at 4°C and eluted in sample buffer (50 mM Tris-HCl pH 6.8, 2% SDS, 10% glycerol, 12.5 mM EDTA, 0.02% bromophenol blue) with final concentration of 2% β-mercaptoethanol and denatured at 95°C for 10 min. Proteins were separated by electrophoresis using Bolt Novex 4–12% gradient Bis-Tris gels (Invitrogen), transferred to Immobilon-P transfer membranes (Millipore Corp) and blocked for 1h in 2% BSA in TBST buffer (10 mM Tris (pH 7.5), 150 mM NaCl, and 0.3% Tween-20). The blocked membranes were incubated overnight at 4°C with primary antibodies (see table 1) in TBST containing 2% BSA, following by 1 h hour incubation at room temperature with horseradish peroxidase–conjugated goat anti-mouse IgG or goat anti-rabbit IgG (diluted 1:5000 in 2% BSA in TBST buffer). After washing, the bound antibodies were detected

by enhanced chemiluminescence using or Clarity™ Western ECL Substrate (Bio-Rad) and signal intensities were quantified using ImageJ [48,49].

Antibodies

Primary antibodies used are listed in Table 1. Secondary antibodies were: donkey anti-rabbit Alexa 594, donkey anti-goat Alexa 594, donkey anti-goat Alexa 647, goat-anti mouse Alexa 647 (Invitrogen), stabilized goat anti-mouse HRP-conjugated and stabilized goat anti-rabbit HRP-conjugated (BioRad).

Antigen	Name	Type	Application	Dilution	Source
Integrin α3		Rabbit pAb	WB	1:2000	Home made
Integrin α3	AF2787	Goat pAb	IF	1:100	R&D
Integrin α3	AF2787	Goat pAb	FACS	1:100	R&D
Integrin α3	sc-374242	Mouse mAb	IHC	1:500	Santa Cruz
Integrin α6-PE	eBioGoH3	Rat mAb	FACS	1:200	eBioscience
CCN2	E-5	Mouse mAb	WB	1:800	Santa Cruz
CCN2	L-20	Goat pAb	IF	1:100	Santa Cruz
CCN2	L-20	Goat pAb	IHC		Santa Cruz
CD34-FITC	RAM34	Rat mAb	FACS	1:100	eBioscience
GAPDH	CB1001	Mouse mAb	WB	1:1000	Calbiochem
GFP	ab6556	Rabbit pAb	IHC	1:2000	Abcam
Keratin 15	MA1-90929	Mouse mAb	IF	1:200	Thermo scientific
Keratin 15	MA1-90929	Mouse mAb	IHC	1:200	Thermo scientific
Ki67	PSX1028	Rabbit pAb	IHC	1:750	Monosan
Laminin-332	R14	Rabbit pAb	IF	1:400	Kind gift of M. Aumailey

Table 1: List of primary antibodies used, including application, dilution and source

Statistical Analysis

Statistical analysis was performed using GraphPad Prism (version 7.0c). Graphs represent the mean and error bars standard deviation (SD) or standard error of mean (SEM), as indicated per graph. Unpaired two-tailed t test was used for comparisons of experimental groups with a control group. One-way ANOVA was used to analyze experiments with more than two groups and two-way ANOVA was performed on experimental data where we investigated the effect of different treatments on two distinct cell types. Type I errors were reduced by testing only planned comparisons among a relatively small number of means. Planned comparisons were conducted using Fisher's Least Significant Difference test after a global ANOVA was determined to be

significant. The significant values shown are described in appropriate figure legends. Results with P value lower than 0.05 were considered significantly different from the null hypothesis.

DATA AVAILABILITY

The RNA sequencing data from this publication have been deposited to the GEO database and assigned the identifier GSE135983.

ACKNOWLEDGMENTS

We would like to acknowledge Alba Zuidema for the help with mouse work and for helpful discussions. We further would like to thank Reinhard Fässler for critical reading of the manuscript and Guoqiang Gu for sharing K19-CreER mice.

REFERENCES

[1] G. Cotsarelis, Epithelial stem cells: a folliculocentric view, J. Invest. Dermatol. 126 (2006) 1459–1468. https://doi.org/10.1038/sj.jid.5700376.

[2] T.S. Purba, I.S. Haslam, E. Poblet, F. Jiménez, A. Gandarillas, A. Izeta, R. Paus, Human epithelial hair follicle stem cells and their progeny: current state of knowledge, the widening gap in translational research and future challenges, Bioessays. 36 (2014) 513–525. https://doi.org/10.1002/bies.201300166.

[3] P. Rompolas, V. Greco, Stem cell dynamics in the hair follicle niche, Semin Cell Dev Biol. 0 (2014) 34–42. https://doi.org/10.1016/j.semcdb.2013.12.005.

[4] M. Ito, Y. Liu, Z. Yang, J. Nguyen, F. Liang, R.J. Morris, G. Cotsarelis, Stem cells in the hair follicle bulge contribute to wound repair but not to homeostasis of the epidermis, Nat. Med. 11 (2005) 1351–1354. https://doi.org/10.1038/nm1328.

[5] A.N. Vagnozzi, J.F. Reiter, S.Y. Wong, Hair follicle and interfollicular epidermal stem cells make varying contributions to wound regeneration, Cell Cycle. 14 (2015) 3408–3417. https://doi.org/10.1080/15384101.2015.1090062.

[6] S. Chen, M. Takahara, M. Kido, S. Takeuchi, H. Uchi, Y. Tu, Y. Moroi, M. Furue, Increased expression of an epidermal stem cell marker, cytokeratin 19, in cutaneous squamous cell carcinoma, Br. J. Dermatol. 159 (2008) 952–955. https://doi.org/10.1111/j.1365-2133.2008.08731.x.

[7] H.C. Kim, S.H. Sohng, D.H. Shin, J.S. Choi, Y.K. Bae, Immunohistochemical expression of cytokeratin 15, cytokeratin 19, follistatin, and Bmi-1 in basal cell carcinoma, Int. J. Dermatol. 55 (2016) 36–44. https://doi.org/10.1111/ijd.12771.

[8] D.J. Kim, K. Kataoka, D. Rao, K. Kiguchi, G. Cotsarelis, J. Digiovanni, Targeted disruption of stat3 reveals a major role for follicular stem cells in skin tumor initiation, Cancer Res. 69 (2009) 7587–7594. https://doi.org/10.1158/0008-5472.CAN-09-1180.

[9] G. Lapouge, K.K. Youssef, B. Vokaer, Y. Achouri, C. Michaux, P.A. Sotiropoulou, C. Blanpain, Identifying the cellular origin of squamous skin tumors, Proc. Natl. Acad. Sci. U.S.A. 108 (2011) 7431–7436. https://doi.org/10.1073/pnas.1012720108.

[10] S. Li, H. Park, C.S. Trempus, D. Gordon, Y. Liu, G. Cotsarelis, R.J. Morris, A keratin 15 containing stem cell population from the hair follicle contributes to squamous papilloma development in the mouse, Molecular Carcinogenesis. 52 (2013) 751–759. https://doi.org/10.1002/mc.21896.

[11] A. Sánchez-Danés, C. Blanpain, Deciphering the cells of origin of squamous cell carcinomas, Nat. Rev. Cancer. 18 (2018) 549–561. https://doi.org/10.1038/s41568-018-0024-5.

[12] V. Ramovs, L. Te Molder, A. Sonnenberg, The opposing roles of laminin-binding integrins in cancer, Matrix Biol. 57–58 (2017) 213–243. https://doi.org/10.1016/j.matbio.2016.08.007.

[13] S. Subbaram, C.M. Dipersio, Integrin α3β1 as a breast cancer target, Expert Opin. Ther. Targets. 15 (2011) 1197–1210. https://doi.org/10.1517/14728222.2011.609557.

[14] N. Sachs, P. Secades, L. van Hulst, M. Kreft, J.-Y. Song, A. Sonnenberg, Loss of integrin α3 prevents skin tumor formation by promoting epidermal turnover and depletion of slow-cycling cells, Proc. Natl. Acad. Sci. U.S.A. 109 (2012) 21468–21473. https://doi.org/10.1073/pnas.1204614110.

[15] G.C. van de Glind, J.J. Out-Luiting, H.G. Rebel, C.P. Tensen, F.R. de Gruijl, Lgr5+ stem cells and their progeny in mouse epidermis under regimens of exogenous skin carcinogenesis, and their absence in ensuing skin tumors, Oncotarget. 7 (2016) 52085–52094. https://doi.org/10.18632/oncotarget.10475.

[16] P.Y. Huang, E. Kandyba, A. Jabouille, J. Sjolund, A. Kumar, K. Halliwill, M. McCreery, R. DelRosario, H.C. Kang, C.E. Wong, J. Seibler, V. Beuger, M. Pellegrino, A. Sciambi, D.J. Eastburn, A. Balmain, Lgr6 is a stem cell marker in mouse skin squamous cell carcinoma, Nat. Genet. 49 (2017) 1624–1632. https://doi.org/10.1038/ng.3957.

[17] T.-C. Troy, A. Arabzadeh, K. Turksen, Re-assessing K15 as an epidermal stem cell marker, Stem Cell Rev. 7 (2011) 927–934. https://doi.org/10.1007/s12015-011-9243-9.
[18] A.L. Means, Y. Xu, A. Zhao, K.C. Ray, G. Gu, A CK19(CreERT) knockin mouse line allows for conditional DNA recombination in epithelial cells in multiple endodermal organs, Genesis. 46 (2008) 318–323. https://doi.org/10.1002/dvg.20397.
[19] M.D. Muzumdar, B. Tasic, K. Miyamichi, L. Li, L. Luo, A global double-fluorescent Cre reporter mouse, Genesis. 45 (2007) 593–605. https://doi.org/10.1002/dvg.20335.
[20] C. Margadant, K. Raymond, M. Kreft, N. Sachs, H. Janssen, A. Sonnenberg, Integrin alpha3beta1 inhibits directional migration and wound re-epithelialization in the skin, J. Cell. Sci. 122 (2009) 278–288. https://doi.org/10.1242/jcs.029108.
[21] M.Q. Reeves, E. Kandyba, S. Harris, R. Del Rosario, A. Balmain, Multicolour lineage tracing reveals clonal dynamics of squamous carcinoma evolution from initiation to metastasis, Nat. Cell Biol. 20 (2018) 699–709. https://doi.org/10.1038/s41556-018-0109-0.
[22] B.A. Diwan, J.M. Ward, J. Henneman, M.L. Wenk, Effects of short-term exposure to the tumor promoter, 12-O-tetradecanoylphorbol-13-acetate on skin carcinogenesis in SENCAR mice, Cancer Lett. 26 (1985) 177–184. https://doi.org/10.1016/0304-3835(85)90024-2.
[23] H. Hennings, R. Shores, P. Mitchell, E.F. Spangler, S.H. Yuspa, Induction of papillomas with a high probability of conversion to malignancy, Carcinogenesis. 6 (1985) 1607–1610. https://doi.org/10.1093/carcin/6.11.1607.
[24] T. Quan, Y. Xu, Z. Qin, P. Robichaud, S. Betcher, K. Calderone, T. He, T.M. Johnson, J.J. Voorhees, G.J. Fisher, Elevated YAP and its downstream targets CCN1 and CCN2 in basal cell carcinoma: impact on keratinocyte proliferation and stromal cell activation, Am. J. Pathol. 184 (2014) 937–943. https://doi.org/10.1016/j.ajpath.2013.12.017.
[25] Y. Ramazani, N. Knops, M.A. Elmonem, T.Q. Nguyen, F.O. Arcolino, L. van den Heuvel, E. Levtchenko, D. Kuypers, R. Goldschmeding, Connective tissue growth factor (CTGF) from basics to clinics, Matrix Biol. 68–69 (2018) 44–66. https://doi.org/10.1016/j.matbio.2018.03.007.
[26] S. Liu, A. Leask, CCN2 modulates hair follicle cycling in mice, Mol. Biol. Cell. 24 (2013) 3939–3944. https://doi.org/10.1091/mbc.E13-08-0472.
[27] L. Rittié, S.W. Stoll, S. Kang, J.J. Voorhees, G.J. Fisher, Hedgehog signaling maintains hair follicle stem cell phenotype in young and aged human skin, Aging Cell. 8 (2009) 738–751. https://doi.org/10.1111/j.1474-9726.2009.00526.x.
[28] B. Ancrile, K.-H. Lim, C.M. Counter, Oncogenic Ras-induced secretion of IL6 is required for tumorigenesis, Genes Dev. 21 (2007) 1714–1719. https://doi.org/10.1101/gad.1549407.
[29] M.V. Plikus, D.L. Gay, E. Treffeisen, A. Wang, R.J. Supapannachart, G. Cotsarelis, Epithelial stem cells and implications for wound repair, Semin. Cell Dev. Biol. 23 (2012) 946–953. https://doi.org/10.1016/j.semcdb.2012.10.001.
[30] R.J. Morris, K.A. Tryson, K.Q. Wu, Evidence that the epidermal targets of carcinogen action are found in the interfollicular epidermis of infundibulum as well as in the hair follicles, Cancer Res. 60 (2000) 226–229.
[31] R.J. Morris, K. Coulter, K. Tryson, S.R. Steinberg, Evidence that cutaneous carcinogen-initiated epithelial cells from mice are quiescent rather than actively cycling, Cancer Res. 57 (1997) 3436–3443.
[32] F.J.A. Conti, R.J. Rudling, A. Robson, K.M. Hodivala-Dilke, alpha3beta1-integrin regulates hair follicle but not interfollicular morphogenesis in adult epidermis, J. Cell. Sci. 116 (2003) 2737–2747. https://doi.org/10.1242/jcs.00475.
[33] G. Lapouge, B. Beck, D. Nassar, C. Dubois, S. Dekoninck, C. Blanpain, Skin squamous cell carcinoma propagating cells increase with tumour progression and invasiveness, EMBO J. 31 (2012) 4563–4575. https://doi.org/10.1038/emboj.2012.312.

[34] I. Malanchi, H. Peinado, D. Kassen, T. Hussenet, D. Metzger, P. Chambon, M. Huber, D. Hohl, A. Cano, W. Birchmeier, J. Huelsken, Cutaneous cancer stem cell maintenance is dependent on beta-catenin signalling, Nature. 452 (2008) 650–653. https://doi.org/10.1038/nature06835.

[35] C.S. Trempus, R.J. Morris, M. Ehinger, A. Elmore, C.D. Bortner, M. Ito, G. Cotsarelis, J.G.W. Nijhof, J. Peckham, N. Flagler, G. Kissling, M.M. Humble, L.C. King, L.D. Adams, D. Desai, S. Amin, R.W. Tennant, CD34 expression by hair follicle stem cells is required for skin tumor development in mice, Cancer Res. 67 (2007) 4173–4181. https://doi.org/10.1158/0008-5472.CAN-06-3128.

[36] A.C. White, K. Tran, J. Khuu, C. Dang, Y. Cui, S.W. Binder, W.E. Lowry, Defining the origins of Ras/p53-mediated squamous cell carcinoma, Proc. Natl. Acad. Sci. U.S.A. 108 (2011) 7425–7430. https://doi.org/10.1073/pnas.1012670108.

[37] J. Goldstein, E. Roth, N. Roberts, R. Zwick, S. Lin, S. Fletcher, A. Tadeu, C. Wu, A. Beck, C. Zeiss, M. Suárez-Fariñas, V. Horsley, Loss of endogenous Nfatc1 reduces the rate of DMBA/TPA-induced skin tumorigenesis, Mol Biol Cell. 26 (2015) 3606–3614. https://doi.org/10.1091/mbc.E15-05-0282.

[38] C.M. Pineda, D.G. Gonzalez, C. Matte-Martone, J. Boucher, E. Lathrop, S. Gallini, N.R. Fons, T. Xin, K. Tai, E. Marsh, D.X. Nguyen, K.C. Suozzi, S. Beronja, V. Greco, Hair follicle regeneration suppresses Ras-driven oncogenic growth, J. Cell Biol. 218 (2019) 3212–3222. https://doi.org/10.1083/jcb.201907178.

[39] T.R. Medler, L.M. Coussens, Duality of the immune response in cancer: lessons learned from skin, J. Invest. Dermatol. 134 (2014) E23-28. https://doi.org/10.1038/skinbio.2014.5.

[40] M. NEAGU, C. CARUNTU, C. CONSTANTIN, D. BODA, S. ZURAC, D.A. SPANDIDOS, A.M. TSATSAKIS, Chemically induced skin carcinogenesis: Updates in experimental models (Review), Oncol Rep. 35 (2016) 2516–2528. https://doi.org/10.3892/or.2016.4683.

[41] J. Zhang, L. Chen, M. Xiao, C. Wang, Z. Qin, FSP1+ fibroblasts promote skin carcinogenesis by maintaining MCP-1-mediated macrophage infiltration and chronic inflammation, Am. J. Pathol. 178 (2011) 382–390. https://doi.org/10.1016/j.ajpath.2010.11.017.

[42] W. Longmate, C.M. DiPersio, Beyond adhesion: emerging roles for integrins in control of the tumor microenvironment, F1000Res. 6 (2017) 1612. https://doi.org/10.12688/f1000research.11877.1.

[43] W.M. Longmate, S.P. Lyons, S.V. Chittur, K.M. Pumiglia, L. Van De Water, C.M. DiPersio, Suppression of integrin α3β1 by α9β1 in the epidermis controls the paracrine resolution of wound angiogenesis, J. Cell Biol. 216 (2017) 1473–1488. https://doi.org/10.1083/jcb.201510042.

[44] K. Mitchell, K.B. Svenson, W.M. Longmate, K. Gkirtzimanaki, R. Sadej, X. Wang, J. Zhao, A.G. Eliopoulos, F. Berditchevski, C.M. Dipersio, Suppression of integrin alpha3beta1 in breast cancer cells reduces cyclooxygenase-2 gene expression and inhibits tumorigenesis, invasion, and cross-talk to endothelial cells, Cancer Res. 70 (2010) 6359–6367. https://doi.org/10.1158/0008-5472.CAN-09-4283.

[45] R. Zheng, W.M. Longmate, L. DeFreest, S. Varney, L. Wu, C.M. DiPersio, L. Van De Water, Keratinocyte integrin α3β1 promotes secretion of IL-1α to effect paracrine regulation of fibroblast gene expression and differentiation, J. Invest. Dermatol. (2019). https://doi.org/10.1016/j.jid.2019.02.025.

[46] G.W. McLean, N.H. Komiyama, B. Serrels, H. Asano, L. Reynolds, F. Conti, K. Hodivala-Dilke, D. Metzger, P. Chambon, S.G.N. Grant, M.C. Frame, Specific deletion of focal adhesion kinase suppresses tumor formation and blocks malignant progression, Genes Dev. 18 (2004) 2998–3003. https://doi.org/10.1101/gad.316304.

[47] R. Pérez-Lorenzo, L.M. Markell, K.A. Hogan, S.H. Yuspa, A.B. Glick, Transforming growth factor β1 enhances tumor promotion in mouse skin carcinogenesis, Carcinogenesis. 31 (2010) 1116–1123. https://doi.org/10.1093/carcin/bgq041.

[48] F. Zanconato, M. Forcato, G. Battilana, L. Azzolin, E. Quaranta, B. Bodega, A. Rosato, S. Bicciato, M. Cordenonsi, S. Piccolo, Genome-wide association between YAP/TAZ/TEAD and AP-1 at enhancers drives oncogenic growth, Nat Cell Biol. 17 (2015) 1218–1227. https://doi.org/10.1038/ncb3216.

[49] S. Sonnylal, S. Xu, H. Jones, A. Tam, V.R. Sreeram, M. Ponticos, J. Norman, P. Agrawal, D. Abraham, B. de Crombrugghe, Connective tissue growth factor causes EMT-like cell fate changes in vivo and in vitro, J. Cell. Sci. 126 (2013) 2164–2175. https://doi.org/10.1242/jcs.111302.

[50] M. Ketema, P. Secades, M. Kreft, L. Nahidiazar, H. Janssen, K. Jalink, J.M. de Pereda, A. Sonnenberg, The rod domain is not essential for the function of plectin in maintaining tissue integrity, Mol Biol Cell. 26 (2015) 2402–2417. https://doi.org/10.1091/mbc.E15-01-0043.

[51] C.T. Rueden, J. Schindelin, M.C. Hiner, B.E. DeZonia, A.E. Walter, E.T. Arena, K.W. Eliceiri, ImageJ2: ImageJ for the next generation of scientific image data, BMC Bioinformatics. 18 (2017) 529. https://doi.org/10.1186/s12859-017-1934-z.

[52] J. Schindelin, I. Arganda-Carreras, E. Frise, V. Kaynig, M. Longair, T. Pietzsch, S. Preibisch, C. Rueden, S. Saalfeld, B. Schmid, J.-Y. Tinevez, D.J. White, V. Hartenstein, K. Eliceiri, P. Tomancak, A. Cardona, Fiji: an open-source platform for biological-image analysis, Nature Methods. 9 (2012) 676–682. https://doi.org/10.1038/nmeth.2019.

[53] K.B. Jensen, R.R. Driskell, F.M. Watt, Assaying proliferation and differentiation capacity of stem cells using disaggregated adult mouse epidermis, Nat Protoc. 5 (2010) 898–911. https://doi.org/10.1038/nprot.2010.39.

[54] T. Harmsen, S. Klaasen, H. van de Vrugt, H. te Riele, DNA mismatch repair and oligonucleotide end-protection promote base-pair substitution distal from a CRISPR/Cas9-induced DNA break, Nucleic Acids Res. 46 (2018) 2945–2955. https://doi.org/10.1093/nar/gky076.

SUPPLEMENTARY FIGURES

Supplementary figure 1

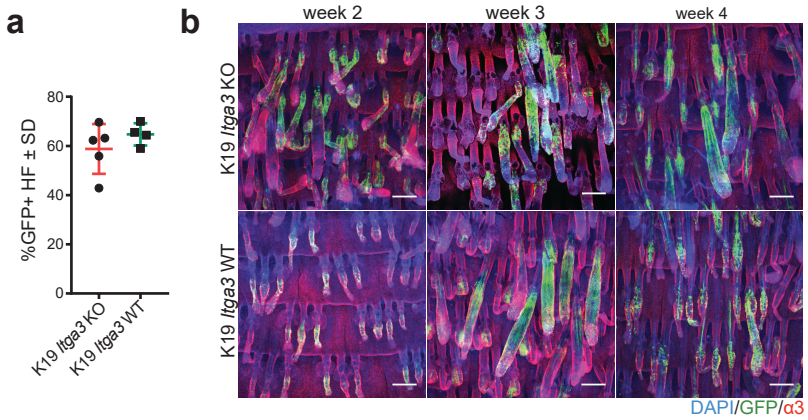

(**a**) Quantification of the percentage of GFP-positive HFs in the back skin of 7-week-old K19 Itga3 KO and WT mice one week after tamoxifen treatment. Each dot represents a mouse (mean ± SD, unpaired t test). (**b**) Linage tracing of GFP-positive HB keratinocytes in K19 Itga3 KO and WT mice at up to four weeks after tamoxifen treatment (whole mounts of tail epidermis, scale bar: 200 μm).

Supplementary figure 2

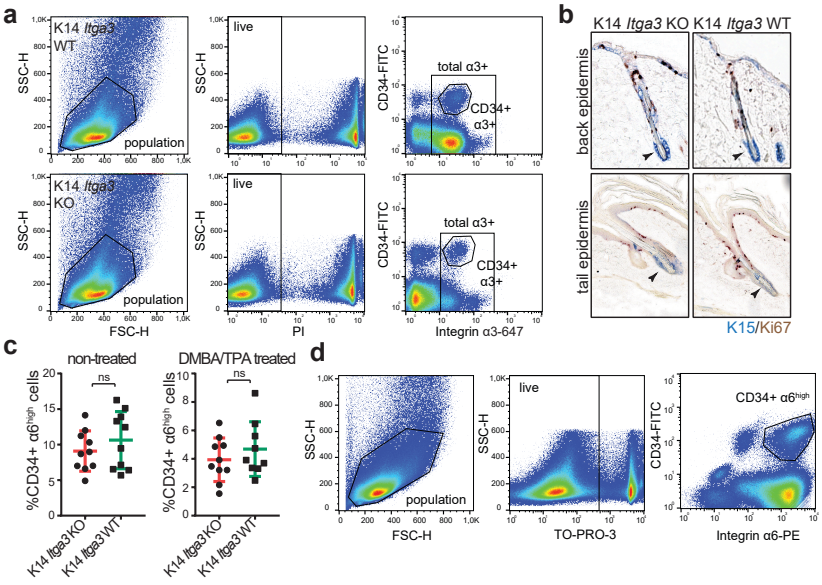

(**a**) Gating strategy of figure 2d. (**b**) Double IHC staining for proliferation marker Ki67 and HB marker K15 shows the absence of proliferation of K15-positive HBs in back and tail epidermis of K14 Itga3 KO and WT mice. (**c**) FACS quantification of the HB population (CD34+, α6high) in the back skin of K14 Itga3 KO and WT mice in homeostatic conditions and after short-term DMBA/TPA treatment (mean ± SD, unpaired t test). (**d**) Gating strategy of Supplementary figure S2c.

Supplementary figure 3

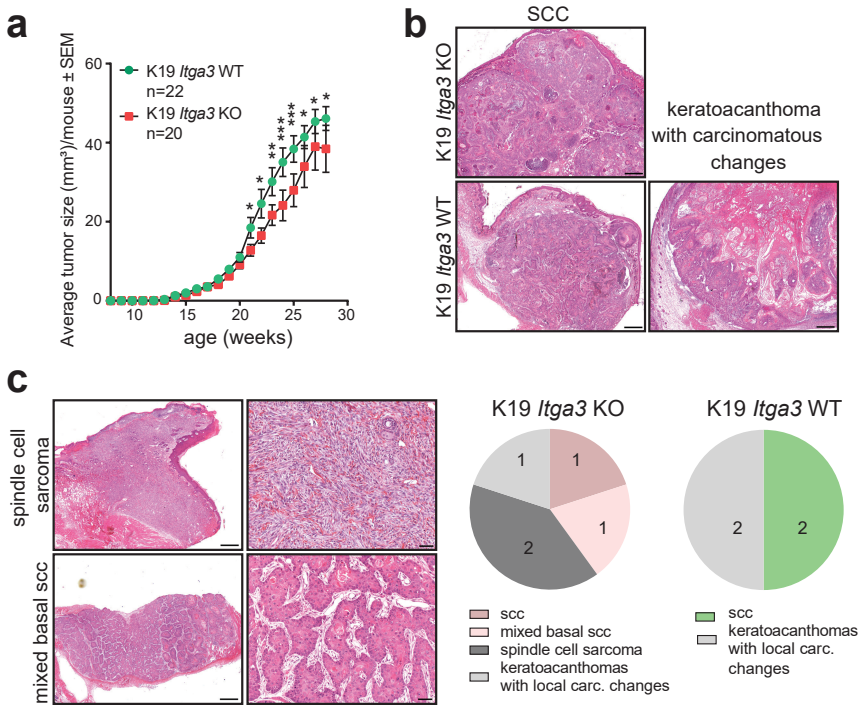

(**a**) The average tumor size is slightly, but significantly decreased in K19 Itga3 KO compared to WT mice submitted to DMBA/TPA-carcinogenesis protocol (mean ± SEM, unpaired t test, *P<0.05, **P<0.005, ***P<0.0005). (**b**) Histology of progressed tumors at the end of DMBA/TPA treatment: SCC, isolated from K19 Itga3 KO and WT mice and keratoacanthomas with carcinomatous changes, isolated from K19 Itga3WT mouse. Progressed tumors were observed in only one K19 Itga3 KO and three WT mice at the end of the treatment. (**c**) Histology (left) and quantification (right) of the progressed tumors of 7 K19 Itga3 KO and 7 WT mice, kept on prolonged TPA treatment for up to additional 10 weeks. 5 K19 Itga3 KO (1 tumor/mouse) and 3 K19 Itga3 WT (1 or 2 tumors/mouse) mice showed tumor progression. In addition to the SCCs and keratoacanthomas with carcinomatous changes, K19 Itga3 KO mice also developed spindle cell sarcomas and mixed basal SCC.

Supplementary figure 4

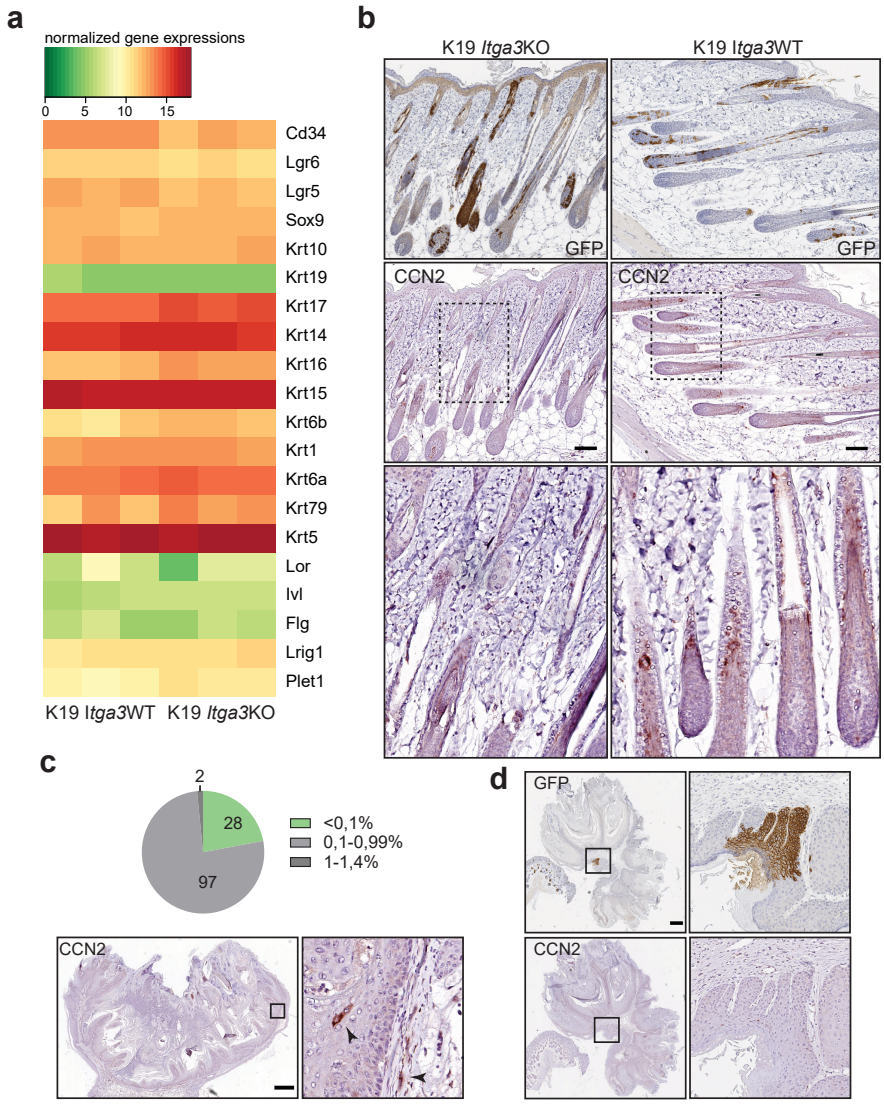

(**a**) A heat map showing expression of selected epidermal markers, selected from gene-list, in GFP-positive HB-originating keratinocytes, isolated from the skin of short-term DMBA/TPA-treated K19 Itga3 KO and WT mice. (**b**) IHC staining for GFP and CCN2 in the skin of short-term DMBA/TPA-treated K19 Itga3 KO and WT mice (scale bar: 100 µm). (**c**) Sparse CCN2-positive cells can be observed in epithelia and stoma of all tumors of K19 Itga3 WT mice (arrow heads). Top: Quantification of the CCN2-positive surface in cross-section of 127 tumors, isolated from 6 K19 Itga3 WT mice. CCN2 represents less than 1% of total tumor surface in the majority of tumors. Bottom: representative IHC staining for CCN2 (scale bar: 500 µm). (**d**) Consecutive section of papilloma, isolated from K19 Itga3 WT mouse, stained for GFP and CCN2. No overlap of the two markers can be observed (scale bar: 500 µm).

Supplementary figure 5

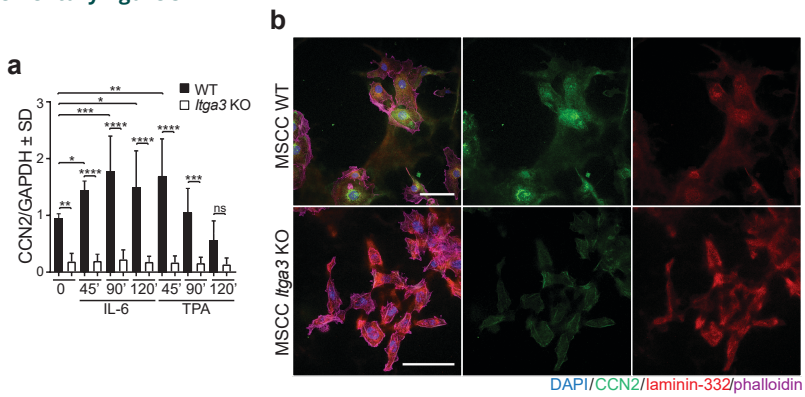

(**a**) Quantification of WB from figure 7c. Bars represent the mean of 5 independent experiments (mean ± SD Fisher's LSD test, *P<0.05, **P<0.005, ***P<0.0005, ****P<0.0001). (**b**) IF images showing co-localization of excreted CCN2 and laminin-332 in the culture of non-treated MSCC Itga3 KO and WT keratinocytes.

Supplementary figure 6

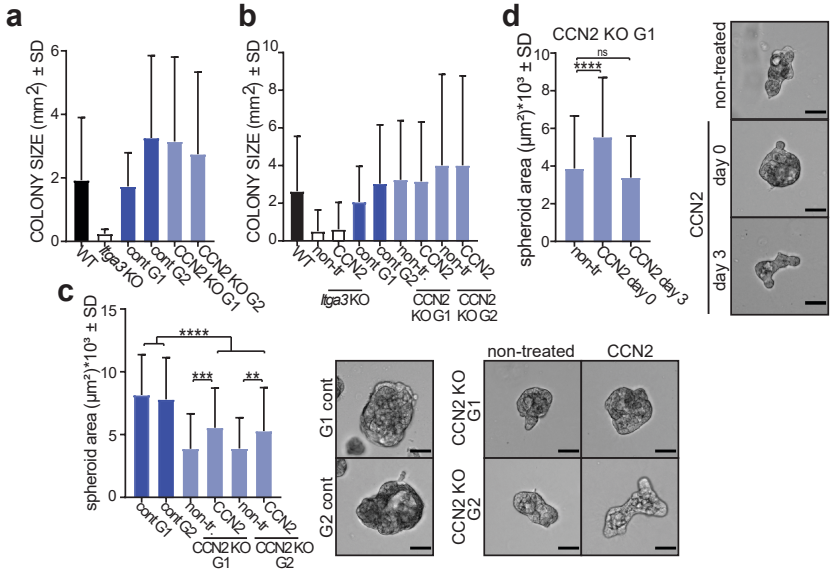

(**a**) Quantification of the colony size from colony formation from figure 8b. Total colonies from 3 independent experiments were quantified (n=246-563, mean ±SD). (**b**) Quantification of the colony size from colony formation from figure c and d. Total colonies from 3 independent experiments were quantified (n=166-779, mean ± SD). (**c**) 3D growth of CCN2 KO MSCC spheroids shows small but significant increase when cells are seeded with 180 ng/ml of CCN2. Left: bright filed images of representative spheroids (scale bar: 50 μm). Right: size quantification of 90 spheroids measured over 3 independent experiments (mean ± SD, Fisher's LSD test, **P<0.005, ***P<0.0005, ****P<0.0001). (**d**) Whereas seeding MSCC CCN2 G1 clone with CCN2 increases its 3D growth, such effect is not observed when exogenous CCN2 (180 ng/ml) is added when spheroids have already formed 3 days after seeding. Left: size quantification of 90 spheroids measured over 2-3 independent experiments (mean ± SD, Fisher's LSD test, ****P<0.0001). Right: bright filed images of representative spheroids (scale bar: 50 μm).